Electrophysiological investigations on the role of retinal HCN channels

A Thesis submitted for the degree of Philosophiæ Doctor by:

Luca Della Santina
(luca.dellasantina@gmail.com)

Under the supervision of:

Prof. Luigi Cervetto

University of Pisa
Dept. of Scienze Fisiologiche
Neuroscienze di Base e dello Sviluppo

March 2009

Had I the heavens embroidered cloths,
Enwrought with golden and silver light,
The blue and the dim and the dark cloths
Of night and light and the half-light,

I would spread the cloths under your feet:
But I, being poor, have only my dreams;
I have spread my dreams under your feet;
Tread softly because you tread on my dreams.

He Wishes For the Cloths of Heaven
William Butler Yeats (1865 ~ 1939)

Declaration

The work described in this thesis is included in the following papers:

Luca Della Santina, Muriel Bouly, Antonella Asta, Gian Carlo Demontis, Luigi Cervetto and Claudia Gargini

Effect of HCN Channel Inhibition on Retinal Morphology and Function in Normal and Dystrophic Rodents.

Submitted to Invest. Ophtalmol. Vis. Sci., manuscript ID: IOVS-09-3680

Lorenzo Cangiano, Claudia Gargini, Luca Della Santina, Gian Carlo Demontis, Luigi Cervetto

High-Pass Filtering of Input Signals by the I_h Current in a Non-Spiking Neuron, the Retinal Rod Bipolar Cell.

PLoS ONE, 2(12):e1327, 2007

Abstract

Hyperpolarization-activated cyclic nucleotide-modulated (HCN) channels are a particular class of voltage-gated ionic channels, mediating the I_f current in the cardiac tissue and I_h in the central nervous system (CNS). They were initially described in cardiac pacemaker cells, where they play a key role in the generation and regulation of cardiac rhythmicity. In the CNS they participate in processes like dendritic integration, network synchronization, long-term potentiation and motor learning. Because of their role in the cardiac tissue, HCN channels reprepresent a target in clinical pharmacology, but a percentage of patients treated with HCN inhibitors report visual side effects. This is possibly due to interaction with HCN channels expressed in the retinal tissue, where all the four HCN isoforms are present. In this thesis the role of HCN channels in visual processing was investigated.

HCN distribution was evaluated in the murine retina using immunohistochemical techniques. The functional role of these channels in retinal signalling was investigated in details, by means of perforated patch clamp recordings from rod bipolar cells (RBCs) in retinal sections, and by non-invasive recording of the electroretinogram (ERG) in rats, wild-type mice and in mice in which the hcn1 gene was deleted (hcn1-ko mice).

RBCs exhibit the HCN-driven I_h current in response to hyperpolarizing voltage steps. When this current is active, the cellular impedance profile has band-pass properties. Application of the selective HCN blocker ZD7288 inhibits I_h, changing the impedance profile to low-pass mode. These effects are predicted by a mathematical model of the RBC where it is assumed that I_h is the only active conductance. The model also predicts that I_h quickens the light response in RBC.

The *in-vivo* inhibition of HCN channels by the organic blocker Ivabradine induces a slight prolongation of the ERG response to weak flashes. At the same time, it triggers a consistent change of the frequency-response relationship from band-pass to low-pass mode, following to both acute or prolonged drug administration; these effects are reversible upon interruption of treatment.

In the hcn1-ko mice line, ERG responses to flashes are prolonged with respect to control mice. In response to sinusoidal stimulation, hcn1-ko mice exhibit a partial attenuation of the band-pass behavior, but not a complete switch to low-pass mode like that induced by the organic channel blocker.

Taken together these data point out the importance of HCN channels in the early steps of rod retinal signalling. This helps in building a framework that may soon allow to explain the role of I_h in visual side effects experienced during the clinical use of HCN inhibitors. In addition, experiments on hcn1-ko mice deliver the first clue that preserving a partial I_h functionality in the retina, may be an effective way to mitigate the side effects these drugs induce on the visual system.

Sommario

I canali attivati dalla iperpolarizzazione e modulati da nucleotidi ciclici (HCN) sono una particolare classe di canali ionici voltaggio-dipendenti, che mediano la corrente I_f nel tessuto cardiaco e la I_h nel sistema nervoso centrale (SNC). Sono stati descritti per la prima volta nelle cellule pacemaker cardiache, dove rivestono un ruolo chiave sia nella generazione che nella regolazione del ritmo cardiaco. Nel SNC essi partecipano in processi quali l'integrazione dendritica, la sincronizzazione delle reti neurali, il potenziamento a lungo termine e la memorizzazione di compiti motori. A causa del loro ruolo cardiaco, i canali HCN rappresentano un target per la farmacologia clinica, ma purtroppo una percentuale dei pazienti trattati con inibitori degli HCN riportano effetti collaterali a livello visivo. Essi sono probabilmente dovuti all'interazione coi canali HCN presenti nella retina, dove sono espresse tutte e quattro le isoforme. Questa tesi indaga il ruolo dei canali HCN nella funzione visiva.

La distribuzione dei canali HCN è stata valutata nella retina murina mediante tecniche immunoistochimiche. Il ruolo funzionale degli stessi nella trasmissione del segnale visivo è stato indagato in dettaglio mediante patch-clamp perforato su cellule bipolari dei bastoncelli (RBC) in sezioni retiniche, e tramite la tecnica non invasiva dell'elettroretinogramma (ERG) in ratti, topi wild type e topi knockout per il gene hcn1 (hcn1-ko).

Le RBC esibiscono la I_h in risposta a step iperpolarizzanti. Laddove questa corrente è attiva, il profilo d'impedenza di queste cellule assume caratteristiche passa-banda. L'applizazione del bloccante HCN selettivo ZD7288 inibisce la I_h, trasformando il profilo d'impedenza in passa-basso. Questi comportamenti vengono predetti da un modello matematico della RBC dove si assume che I_h sia l'unica conduttanza di tipo attivo. Il modello predice anche che l'I_h è capace di accelerare la risposta alla luce nelle RBC.

L'inibizione dei canali HCN *in-vivo* mediante somministrazione del bloccante Ivabradine induce un leggero prolungamento della risposta a flash di bassa intensità luminosa. Allo stesso tempo provoca una consistente modifica della relazione frequenza - ristposta da un profilo passa-banda ad uno passa-basso, sia a seguito di somministrazione acuta che prolungata; questi effetti sono reversibili mediante interruzione del trattamento.

Nei topi hcn1-ko le risposte ERG da flash si presentano prolungate rispetto agli animali di controllo. In risposta a stimoli sinusoidali la delezione di hcn1 provoca una parziale attenuazione del comportamento passa banda, senza arrivare però ad un comportamento passa-basso come osservato dopo somministrazione del bloccante organico.

Considerati nel loro insieme, questi dati mettono in luce l'importanza dei canali HCN nei primi stadi della trasmissione del segnale visivo dei bastoncelli. Fornendo così un bagaglio di conoscenze che presto potrebbe spiegare il ruolo della I_h negli effetti collaterali riportati durante l'uso clinico degli inibitori dei canali HCN. Gli esprimenti sugli hcn1-ko, inoltre, rappresentano la prima prova che il preservare anche una parziale funzionalità della I_h nella retina, possa essere una buona strategia da seguire per mitigare gli effetti collaterali che questi farmaci provocano a livello visivo.

Contents

List of Figures

Chapter 1

Introduction

> *Any road followed precisely to its end leads precisely nowhere.*
> *Climb the mountain just a little bit to test that it's a mountain.*
> *From the top of the mountain, you cannot see the mountain.*
>
> Family Commentaries by the Princess Irulan

1.1 Retina

1.1.1 Morphological structure of the retina

Among the five senses, vision is especially important in human beings since most of the perceptual experience starts by looking to the external world. The eye is dedicated to capture light reflected by the scene surrounding the subject, to encode it into electrical signals and efficiently transfer them to the brain. At first approximation the eye takes the shape of a sphere, in which the neural portion, the retina, is placed in the backmost hemisphere.

Like many other structures in the central nervous system, a vertical section of the retina reveals an organization structured into morphological and functional layers. From the outmost to the innermost with respect to the ocular bulb's surface they are:

- Pigmented epithelium (PE): Placed at the very periphery of the retina, these highly pigmented cells prevents residual light from scattering back into the photosensitive retina and are involved in key processes like phagocytosis of aged photoreceptor's outer segments and in regeneration of the light-sensitive pigment.

- Photoreceptors' outer segments (OS): The most distal part of photoreceptors where the multi-stage process known as phototransduction begins with the light-induced isomerization of a pigment tightly packed into vesicles (cones) or membrane invaginations (rods). The whole phototransductive machinery is contained in here.

- Photoreceptor's inner segments (IS): Connected to the outer segment by a thin cilium, it is the portion of the cell where most of the biosynthetic processes take place.

- Outer nuclear layer (ONL): Contain all the photoreceptor nuclei, as well as the terminal processes of Müller glia.
- Outer plexiform layer (OPL): Zone of synaptical contact between photoreceptors and second-order neurons
- Inner nuclear layer (INL): In this layer resides the cellular bodies of all the second-order neurons: rod- and cone-bipolar cells, amacrine cells, horizontal cells; and also the non-neural Müller glia.
- Inner plexiform layer (IPL): Zone of synaptical contact between second-order neurons and ganglion cells.
- Ganglion cell layer (GCL): Ganglion cell and displaced amacrine cellular bodies reside in this layer. The former represents the third-order neurons, the only neurons generating spike potentials.
- Optic nerve fiber layer (NFL): Here axons of ganglion cells, packed together, make their way out of the retina toward the brain. Together they form the optic nerve, which at the level of optic disc assumes the usual myelination.

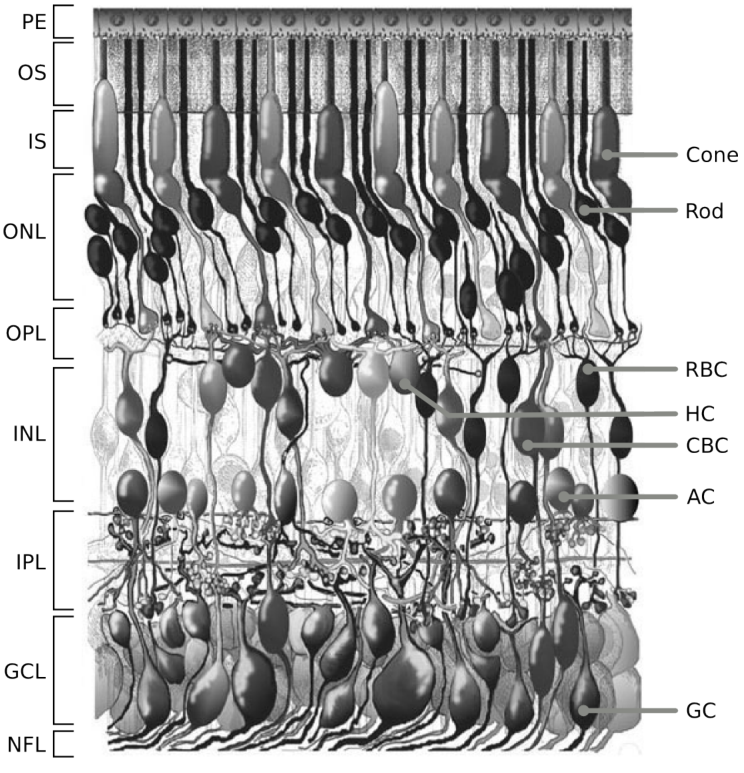

Figure 1.1: Morphological representation of the retina in a vertical section of the adult human eye. Retinal layers on the left. Principal neuronal classes on the right. RBC: rod bipolar cell, HC: horizontal cell, CBC: cone bipolar cell, AC: amacrine cell, GC: ganglion cell

1.1.2 Features of the visual systems of mouse and rat

Mice (*Mus musculus*) and rats (*Rattus norvegicus*) are currently among the most widely used animal species in vision research, especially since the availability of knockout mice lines reproducing phenotypical and/or genotypical features of human pathologies. Despite the great usefulness of these models, some major differences between the visual system of rodents and that of humans must be taken into account during design and interpretation of the experimental work.

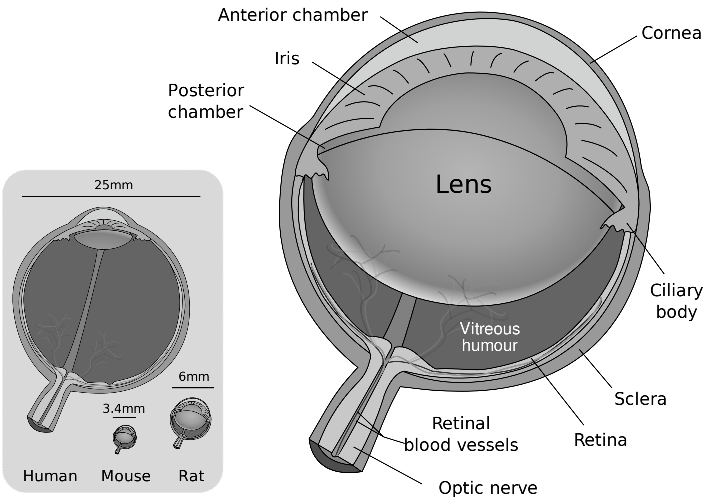

Figure 1.2: Schematic representation of murine eye. Inset: Relative proportion of the eye of human, rat and mouse (image adapted from wikimedia, original author Rhcastillos)

With respect to human eye, the one of rats and mice is quite smaller, respectively 1/4 and 1/7 in diameter. The general structure remains quite similar but the relative proportion of components varies among species. The cornea and lens of mice and rats takes about 60% of the axial eye length [88]. Both mice and rats are nocturnal rodents with laterally-positioned eyes, leading to a small amount of intersection in their monocular visual fields compared to diurnal species with frontally-positioned eyes, yielding a binocular field of about 30-40° (fig. 1.3). Accordingly, the relative proportion of ipsilaterally projecting retinal ganglion cells is small: 2-3% in mice and 3% in rats, compared to 25-30% of cats or 40% of macaques [11].

The retina of these two rodents is strongly rod-dominated (∼97% of photoreceptors are rods in mice, ∼99% in rats), tuning vision for a mostly nocturnal activity. The small population of cones contain two kind of visual pigment, one maximally sensitive to ultraviolet (UV) light (peak at 360 nm) while the other one maximally sensitive to medium(M)-wavelength light (peak at 508 nm) [75]. The dorsal retina exhibits the highest density of M-cones while in the ventral retina UV-cones prevail [99]. In rats only 7% of all cones are UV-sensitive, evenly distributed in their retina [98]. The majority of cones in mice has both pigments, being anyway maximally sensitive to 360nm light.

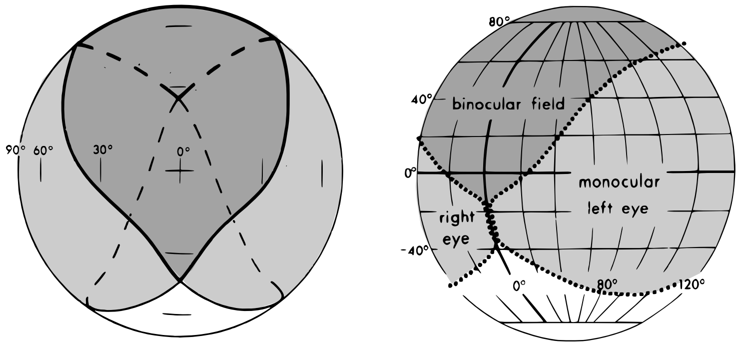

Rat

Mouse

Figure 1.3: Visual field in mice and rats, assuming the animal is sitting in the center of the sphere facing the zero intersection of horizontal and vertical meridians. Schematics for rat and mouse respectively from [45] and [23].

In mice and rats, the neural network carrying the visual signal from photoreceptors to ganglion cells resembles the one of other mammals. For rods, three possible pathways have been described, likely to operate under different light conditions:

- Signal from rods is passed to the unique class of rod bipolar cell (see fig. 1.4). RBCs make synapses with A2 amacrine cells which plug the signal into the evolutionary preexisting cone pathway, by making sign-inverting synapses with OFF cone bipolars and sign-preserving synapes with ON cone bipolars. Cone bipolars carry the signal directly to ganglion cells.
- Rod signal can be passed via gap junctions to cones and thus use the preexisting cone-processing network.
- Rods can make direct synaptic contact with one type of OFF bipolar cells, described as a pathway for driving scotopic signals to OFF ganglion cells by [102].

Cones make synapses with cone bipolar cells (CBCs), which directly contact ganglion cells. Nine subtypes of CBCs are known at the present time (see fig. 1.4) each one characterized by a peculiar morphology and a precise axonal stratification into the IPL. Thus generating an OFF and ON pathway, optimized to process decrements or increments of light. CBCs with axons stratifying within the first two fifth of the IPL belong to the OFF pathway and they functionally present light-evoked hyperpolarizing responses; while those one stratifying in the remaining three fifth belong to the ON pathway and depolarize in response to light stimulation, just like rod bipolar cells.

The relative density of neurones in the murine retina decreases from the most central portion of the retina to the periphery. Rods account for the majority of cells in the murine retina (near 6.4 millions, 97.2% of photoreceptors), while cones are near 180.000 (see fig.1.5). Inside the INL, the relative proportion is quite conserved among species: in mice 41% of cell bodies are bipolar cells, 39% are amacrine, 16% Müller cells and only 3% are horizontal cells. Inside

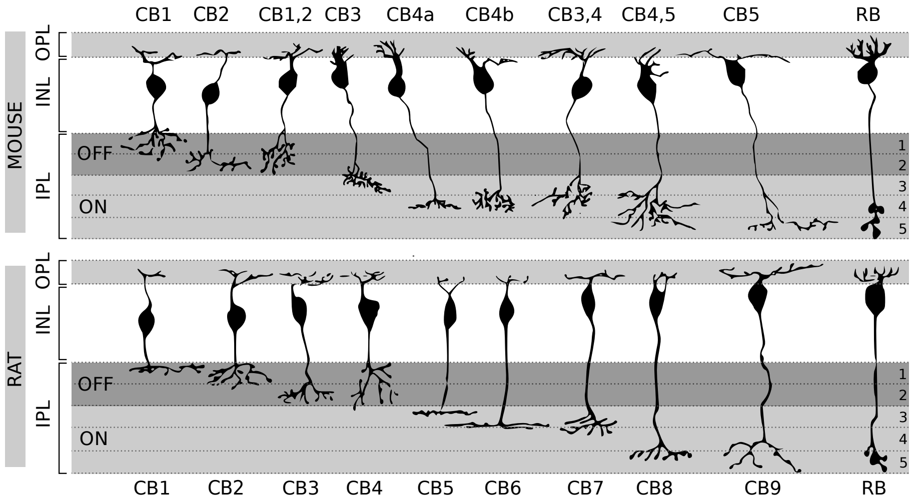

Figure 1.4: Type of bipolar cells in the murine (upper panel) and rat's (lower panel) retina. CB: Cone Bipolar, RB: Rod Bipolar. In dark gray the outmost 2/5 of IPL also known as *sublamina a*. Below, in light gray the *sublamina b*. Image adapted from [84] (mouse) and [37] (rat).

the ganglion cell layer, the majority of cells are displaced amacrine cells (59%) while the remaining 41% are proper ganglion cells [52].

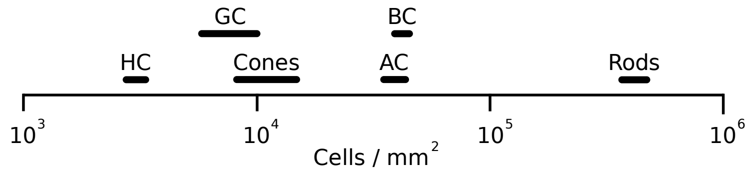

Figure 1.5: Cellular density in the murine retina: for each cell class values are expressed as range spanning from the less populated portion (around the retinal perimeter) to the most populated (in the neighborhood of the optic disc). BC: Bipolar Cells, AC: Amacrine Cells, GC: Ganglion Cells HC: Horizontal Cells. Population data from [52].

Retinal ganglion cells (RGCs) in mice have a very heterogeneous morphology, at present time up to 14 different classes of RGC were identified in the murine retina basing on cellular dimension, morphology and dendritic stratification in the IPL [97], [14]. RGCs receive visual input from cone bipolar cells, in majority as input from both UV- and M-cones, 18% only from UV-cones and a 3% only from M-cones. Around 2% of RGC receive input from UV- and M- cones whose pathway has opposite polarity (ON and OFF) [25], thus representing a possible way to carry chromatic information in these animals. Some ON and ON-OFF ganglion cells exhibit a preferential response to the movement's direction a visual stimulus is presented within their receptive field. These direction-selective RGC were firstly described in the rabbit [81], but recently also identified in the murine retina [107]. A non-image forming class of RGC was discovered in the retina of both mice and rats, but also identified in cats and humans [42] [16] [92]. This class of ganglion cells is intrinsically sensitive to light since these neurons contain an opsin-like pigment, named melanopsin. These RGCs project their axons to the suprachiasmatic nucleus, and are involved in the regulation of circadian rhythms as well as pupillary reflexes. The number of melanopsin RGCs is about 700 cells in the mouse retina and 2300-2600 in the rat's (corresponding to 2.3% of the total number of RGCs).

1.2 HCN channels

1.2.1 Molecular properties of HCN channels

Hyperpolarization-activated, cyclic Nucleotide-modulated (HCN) channels belong to the family of voltage-gated potassium channels (for a review see [72] [2] [112]). In this respect they share a common general membrane topology comprising six transmembrane segments (S1-S6), a signature sequence placed in the loop between S4 and S5 is shared with minor variations among all the channels belonging to this family. In the H5 loop resides the pore-forming region. The S4 segment presents every three or four hydrophobic aminoacids a lysine or arginine; which are positively charged at physiological pH and act as voltage sensor. N- and C-terminals reside in the intracellular membrane side; while in proximity to the first transmembrane segment, close to the intracellular side, a T1 region acts as anchor point for multimeric assembly of the complete channel.

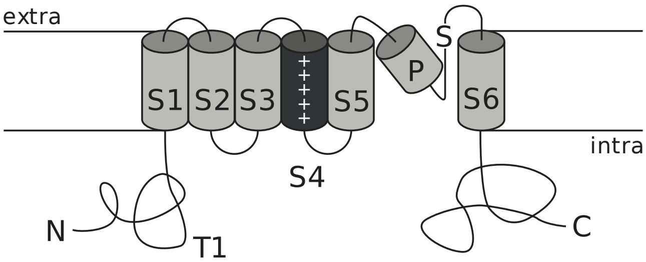

Figure 1.6: General structure of voltage-gated potassium channels. S1-S6: transmembrane segments, P: pore-forming region, S: signature sequence, T1: region involved in subunit assembly. Figure adapted from [72].

HCN channels have all these features common to their superfamily, plus a cytoplasmic region placed between S6 and the C-terminal, which acts as cyclic nucleotide binding domain (CNBD) (fig. 1.7), capable of binding cAMP and cGMP (the latter with less affinity), that act as modulators on channel properties. The CNBD is connected to the S6 segment by an α-helical linker region. The carboxyl terminal portion of the protein, downstream to the CNBD, is also involved in trafficking toward the cellular membrane; HCN channels can distribute in a non-uniform manner along the cellular membrane by interacting via PDZ-binding domain with scaffold proteins like Tamalin, S-SCAM, Mint2 and Filamin A [55] [38]. The complete HCN channel is formed by homo- or hetero-tetramerization of four subunits, which also contribute together in defining the pore region. At present time, four genes are known to code for HCN1-4 channel subunit isoforms in mammals [62] [63]. These four subunits present high level of similarity in the portion enclosed between the beginning of S1 and the end of the CNBD, with the majority of differences localized in correspondence of N- and C-terminals. This evidence suggests that HCN subtypes arose from early duplication of a single ancestral gene [51] and subsequently differentiated during evolution.

Analysis of conserved aminoacid residues among murine HCN channels confirms the common traits of the ancestor family and points out some interesting similarities (fig. 1.8). Transmembrane domains and H5 loop (involved in poreformation) are the most preserved regions. Also their CNBDs present an high percentage of homology, even if some isoform-specific residues are expressed in the median and terminal portion, possibly being the molecular origin for the different sensibility to cyclic nucleotide modulation. A 52 aminoacid portion present at the N-terminal is implied in subunit tetramerization, since its lacking results in a non-functional protein which remains localized in the perinuclear region, instead of being correctly trafficked to membrane [101]. The most variable portions are the N- and C-termini also in mice.

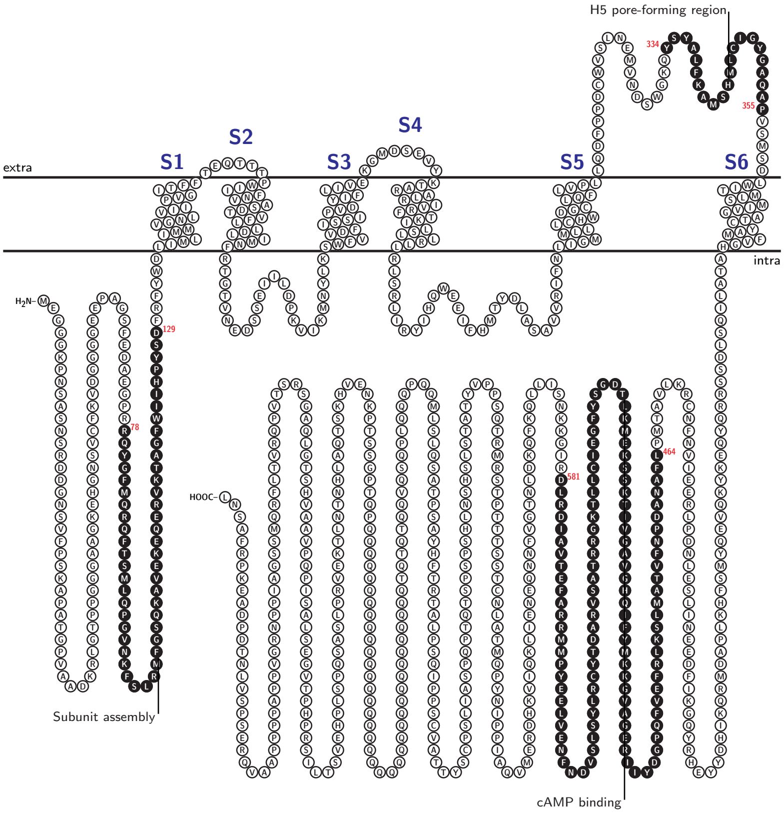

Figure 1.7: Structure of murine HCN1 channel (910 AA). Protein data from UniProtKB/Swiss-Prot, sequence id: O88704. Membrane topology rendered with TEXtopo [6]

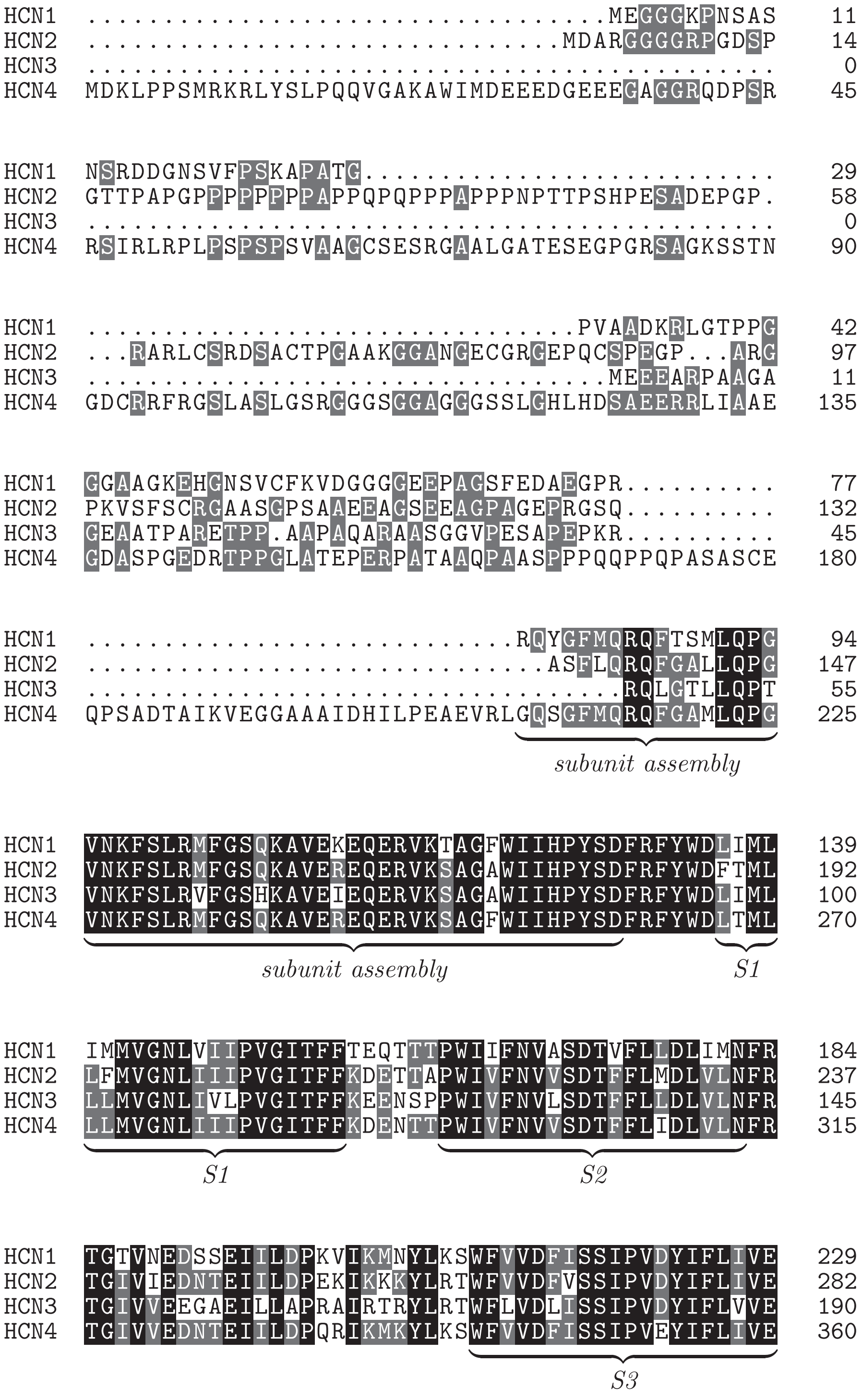

```
HCN1  ..................................MEGGGKPNSAS    11
HCN2  ...............................MDARGGGGRPGDSP    14
HCN3  .............................................     0
HCN4  MDKLPPSMRKRLYSLPQQVGAKAWIMDEEEDGEEEGAGGRQDPSR    45

HCN1  NSRDDGNSVFPSKAPATG...........................    29
HCN2  GTTPAPGPPPPPPPPAPPQPQPPPAPPPNPTTPSHPESADEPGP.    58
HCN3  .............................................     0
HCN4  RSIRLRPLPSPSPSVAAGCSESRGAALGATESEGPGRSAGKSSTN    90

HCN1  ................................PVAADKRLGTPPG    42
HCN2  ...RARLCSRDSACTPGAAKGGANGECGRGEPQCSPEGP...ARG    97
HCN3  ..................................MEEEARPAAGA    11
HCN4  GDCRRFRGSLASLGSRGGGSGGAGGGSSLGHLHDSAEERRLIAAE   135

HCN1  GGAAGKEHGNSVCFKVDGGGGEEPAGSFEDAEGPR..........    77
HCN2  PKVSFSCRGAASGPSAAEEAGSEEAGPAGEPRGSQ..........   132
HCN3  GEAATPARETPP.AAPAQARAASGGVPESAPEPKR..........    45
HCN4  GDASPGEDRTPPGLATEPERPATAAQPAASPPPQQPPQPASASCE   180

HCN1  ............................RQYGFMQRQFTSMLQPG    94
HCN2  ..............................ASFLQRQFGALLQPG   147
HCN3  ...................................RQLGTLLQPT    55
HCN4  QPSADTAIKVEGGAAAIDHILPEAEVRLGQSGFMQRQFGAMLQPG   225

HCN1  VNKFSLRMFGSQKAVEKEQERVKTAGFWIIHPYSDFRFYWDLIML   139
HCN2  VNKFSLRMFGSQKAVEREQERVKSAGAWIIHPYSDFRFYWDFTML   192
HCN3  VNKFSLRVFGSHKAVEIEQERVKSAGAWIIHPYSDFRFYWDLIML   100
HCN4  VNKFSLRMFGSQKAVEREQERVKSAGFWIIHPYSDFRFYWDLTML   270

HCN1  IMMVGNLVIIPVGITFFTEQTTTPWIIFNVASDTVFLLDLIMNFR   184
HCN2  LFMVGNLIIIPVGITFFKDETTAPWIVFNVVSDTFFLMDLVLNFR   237
HCN3  LLMVGNLIVLPVGITFFKEENSPPWIVFNVLSDTFFLLDLVLNFR   145
HCN4  LLMVGNLIIIPVGITFFKDENTTPWIVFNVVSDTFFLIDLVLNFR   315

HCN1  TGTVNEDSSEIILDPKVIKMNYLKSWFVVDFISSIPVDYIFLIVE   229
HCN2  TGIVIEDNTEIILDPEKIKKKYLRTWFVVDFVSSIPVDYIFLIVE   282
HCN3  TGIVVEEGAEILLAPRAIRTRYLRTWFLVDLISSIPVDYIFLVVE   190
HCN4  TGIVVEDNTEIILDPQRIKMKYLKSWFVVDFISSIPVEYIFLIVE   360
```

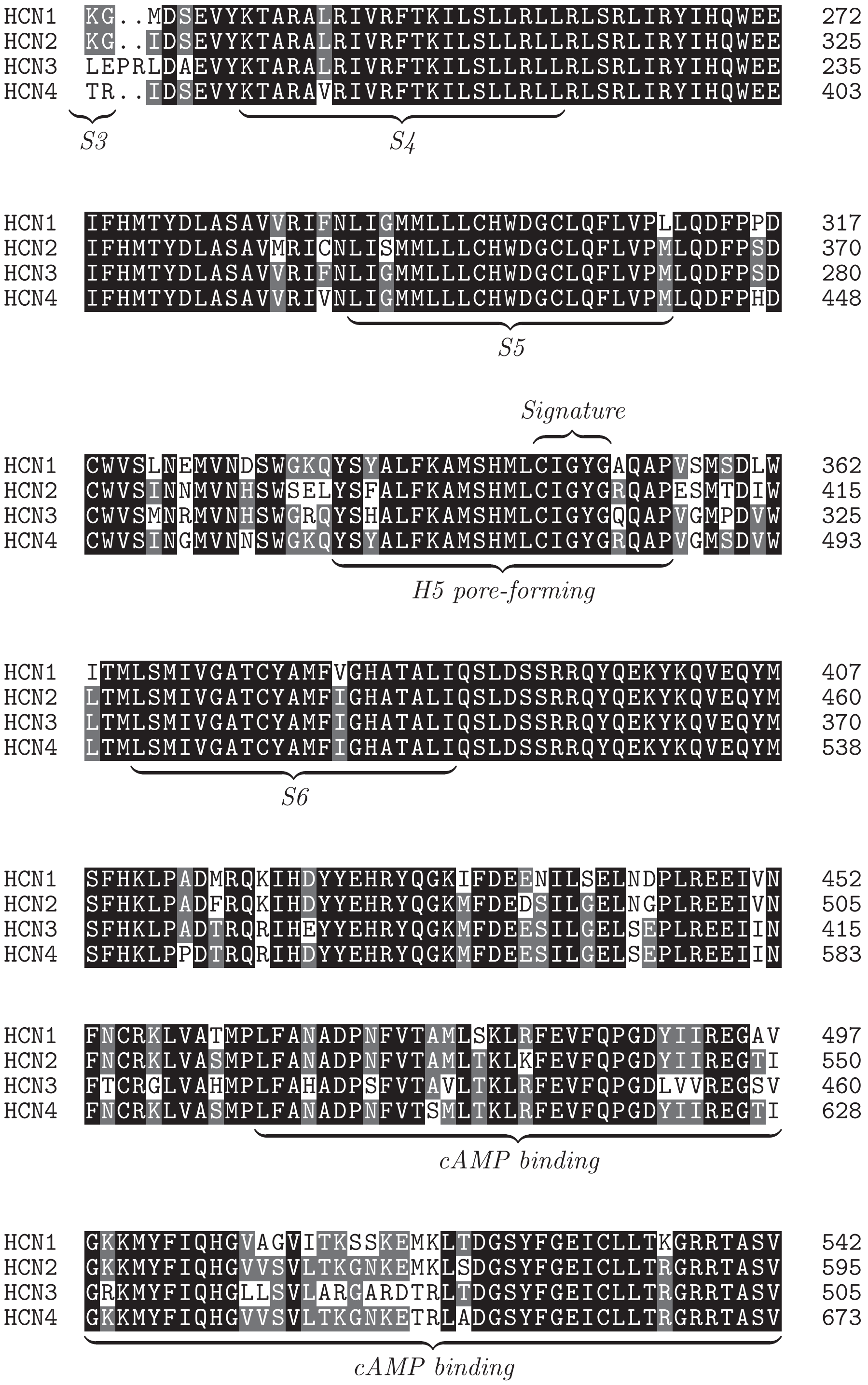

```
HCN1  KG..MDSEVYKTARALRIVRFTKILSLLRLLRLSRLIRYIHQWEE  272
HCN2  KG..IDSEVYKTARALRIVRFTKILSLLRLLRLSRLIRYIHQWEE  325
HCN3  LEPRLDAEVYKTARALRIVRFTKILSLLRLLRLSRLIRYIHQWEE  235
HCN4  TR..IDSEVYKTARAVRIVRFTKILSLLRLLRLSRLIRYIHQWEE  403
```

S3 *S4*

```
HCN1  IFHMTYDLASAVVRIFNLIGMMLLLCHWDGCLQFLVPLLQDFPPD  317
HCN2  IFHMTYDLASAVMRICNLISMMLLLCHWDGCLQFLVPMLQDFPSD  370
HCN3  IFHMTYDLASAVVRIFNLIGMMLLLCHWDGCLQFLVPMLQDFPSD  280
HCN4  IFHMTYDLASAVVRIVNLIGMMLLLCHWDGCLQFLVPMLQDFPHD  448
```

S5

Signature

```
HCN1  CWVSLNEMVNDSWGKQYSYALFKAMSHMLCIGYGAQAPVSMSDLW  362
HCN2  CWVSINNMVNHSWSELYSFALFKAMSHMLCIGYGRQAPESMTDIW  415
HCN3  CWVSMNRMVNHSWGRQYSHALFKAMSHMLCIGYGQQAPVGMPDVW  325
HCN4  CWVSINGMVNNSWGKQYSYALFKAMSHMLCIGYGRQAPVGMSDVW  493
```

H5 pore-forming

```
HCN1  ITMLSMIVGATCYAMFVGHATALIQSLDSSRRQYQEKYKQVEQYM  407
HCN2  LTMLSMIVGATCYAMFIGHATALIQSLDSSRRQYQEKYKQVEQYM  460
HCN3  LTMLSMIVGATCYAMFIGHATALIQSLDSSRRQYQEKYKQVEQYM  370
HCN4  LTMLSMIVGATCYAMFIGHATALIQSLDSSRRQYQEKYKQVEQYM  538
```

S6

```
HCN1  SFHKLPADMRQKIHDYYEHRYQGKIFDEENILSELNDPLREEIVN  452
HCN2  SFHKLPADFRQKIHDYYEHRYQGKMFDEDSILGELNGPLREEIVN  505
HCN3  SFHKLPADTRQRIHEYYEHRYQGKMFDEESILGELSEPLREEIIN  415
HCN4  SFHKLPPDTRQRIHDYYEHRYQGKMFDEESILGELSEPLREEIIN  583
```

```
HCN1  FNCRKLVATMPLFANADPNFVTAMLSKLRFEVFQPGDYIIREGAV  497
HCN2  FNCRKLVASMPLFANADPNFVTAMLTKLKFEVFQPGDYIIREGTI  550
HCN3  FTCRGLVAHMPLFAHADPSFVTAVLTKLRFEVFQPGDLVVREGSV  460
HCN4  FNCRKLVASMPLFANADPNFVTSMLTKLRFEVFQPGDYIIREGTI  628
```

cAMP binding

```
HCN1  GKKMYFIQHGVAGVITKSSKEMKLTDGSYFGEICLLTKGRRTASV  542
HCN2  GKKMYFIQHGVVSVLTKGNKEMKLSDGSYFGEICLLTRGRRTASV  595
HCN3  GRKMYFIQHGLLSVLARGARDTRLTDGSYFGEICLLTRGRRTASV  505
HCN4  GKKMYFIQHGVVSVLTKGNKETRLADGSYFGEICLLTRGRRTASV  673
```

cAMP binding

```
HCN1  RADTYCRLYSLSVDNFNEVLEEYPMMRRAFETVAIDRLDRIGKKN   587
HCN2  RADTYCRLYSLSVDNFNEVLEEYPMMRRAFETVAIDRLDRIGKKN   640
HCN3  RADTYCRLYSLSVDHFNAVLEEFPMMRRAFETVAMDRLRRIGKKN   550
HCN4  RADTYCRLYSLSVDNFNEVLEEYPMMRKKNSILLHKVQHDLN..S   716
                    cAMP binding

HCN1  SILLQKFQKDLNTGVFNNQENEILKQIVKHDREMVQAIPPINYPQ   632
HCN2  SILLHKVQHDLSSGVFNNQENAIIQEIVKYDREMVQQAE.LGQRV   684
HCN3  SILQRKRSEPSPG....SSGGVMEQHLVQHDRDMARGVRGLAPGT   591
HCN4  GVFNYQENE.............IIQQIVRHDREMAHCAHRVQAAA   748

HCN1  MTALNCTSSTTTPTSRMRTQSPPVYTATSLSHSNLHS........   669
HCN2  GLFPPPPPPQVTSAIATLQQAVAMSFCPQVARPLVG.........   720
HCN3  GARLSGKPVLWEPLVHAPLQAAAVTSNVAIALTHQR.........   627
HCN4  SATPTPTPVIWTPLIQAPLQAAAATTSVAIALTHHPRLPAAIFRP   793

HCN1  .............................................   669
HCN2  .............................................   720
HCN3  .............................................   627
HCN4  PPGPGLGNLGAGQTPRHPRRLQSLIPSALGSASPASSPSQVDTPS   838

HCN1  .................PSPSTQTPQPSAILSPCSYTTAVCSPPI   697
HCN2  ...................PLALGS....................   726
HCN3  ................GPLPLSPDS................PATL   640
HCN4  SSSFHIQQLAGFSAPPGLSPLLPSSSSSPPPGACGSPPAPTPSTS   883

HCN1  QSPLATRT.............................FHYASPTA   713
HCN2  .PRLVRRA...................................PP   735
HCN3  LARSARRS................................AGSPA   653
HCN4  TAAAASTTGFGHFHKALGGSLSSSDSPLLTPLQPGARSPQAAQPP   928

HCN1  SQLSLMQQPQQQLPQSQVQQTQTQTQQQQQQQQQQQQ........   750
HCN2  GPLPPAASP.........GPPAASPPAAPSS..............   757
HCN3  SPLVPVRAG..........PLLARGPWASTSRLPAPP........   680
HCN4  PPLPGARGGLGLLEHFLPPPPSSRSPSSSPGQLGQPPGELSLGLA   973

HCN1  .........................................QQQQ   754
HCN2  .............................................   757
HCN3  .............................................   680
HCN4  AGPSSTPETPPRPERPSFMAGASGGASPVAFTPRGGLSPPGHSPG  1018

HCN1  QQQQQQQQQQQQQQQQQQQQQPQTPGSSTPKNEVHKSTQALHNTN   799
HCN2  .PRAPRTSPYGVPGSPATRVGP..ALPARRLSR..ASRP......   791
HCN3  .ARTLHASLSRTGRSQVSLLGPPPGGARRLGP..RGRP......   716
HCN4  PPRTFPSAPPRASGSHGSLLLPPASSPPPPQVPQRRGTPPLTPGR  1063
```

```
HCN1  LTKEVRPLSASQPSLPHEVSTLISRPHPTVGESLASIPQPVAAVH   844
HCN2  .......LSASQPSLPHG.....................VPAPSP   808
HCN3  .......LSASQPSLPQR........................ATG   730
HCN4  LTQDLKLISASQPALPQDGAQTLRRASPHSSGESVAAFSLYPRAG  1108

HCN1  STGLQAGS........RSTVPQRVTLFRQMSSGAIPPNRGVPPAP   881
HCN2  AAS.......................ARPASSSTPRLGPAPTART   830
HCN3  DGS.......................PRRKGSGSERLPPSGLLAK   752
HCN4  GGSGSSGGLGPPGRPYGAIPGQHVTLPRKTSSGSLPPPLSLFGAR  1153

HCN1  PPPAAVQRESPSVLNTDP....DAEKPRFASNL   910
HCN2  AAPSPDRRDSASPGAASGLDPLDSARSRLSSNL   863
HCN3  PPGTVQPPRSSVP...EP...VTPRGPQISANM   779
HCN4  AASSGGPPLTTAAPQREPGARSEPVRSKLPSNL  1186
```

Figure 1.8: Conserved regions in murine HCN channel isoforms. Protein data from UniProtKB/Swiss-Prot, sequence id: O88704 (HCN1), O88703 (HCN2), O88705 (HCN3), O70507 (HCN4). Residue alignment performed with ClustalW 2.0.10. Similarity shading rendered with TeXshade[5], gray shading for conserved residues, black shading for completely matching regions.

1.2.2 I_h current properties

HCN channels have the peculiar feature to be opened in response to an hyperpolarizing stimulus. When this event happens a slowly activating, non-inactivating ionic current flows; this current takes the name of I_f in the cardiac district or I_h in the central nervous system (CNS). I_h exhibits both time- and voltage-dependency and drives a cationic flow across the membrane, mainly sodium and potassium flow with a relative permeability of 1:3 [108], causing an influx of positive charges into the cell, which leads to a depolarization. In case I_h is active at resting potential, this negative feedback mechanism is effective also with depolarizing stimuli, since the induced depolarization of the cellular membrane closes HCN channels, resulting in a hyperpolarization that counteracts the disturbing stimulus.

A major component of this stabilizing effect is due to I_h's voltage-dependant gating: opposite to voltage-gated calcium or sodium channels which are maximally activated at their reversal potential, I_h activation curve falls in its basal values close to the reversal potential, endowing this current with intrinsically negative feedback properties. Activation kinetics depend upon the isoform combination in the tetramer, for homomeric channels kinetics slow down according to: $HCN1 > HCN2 > HCN3 > HCN4$ from a few millisecond for the faster isoform to hundreds of milliseconds and even seconds for the slowest one (at voltages more negative than -100 mV) [32].

HCN channels may be modulated by cyclic nucleotides; in the presence of cAMP and cGMP (the latter with lesser affinity), activation kinetics speed up and the activation curve of these channels is shifted toward more positive potentials. The same shift occurs in the absence of CNBD, suggesting that the CNBD acts by limiting channel kinetics, and this constrain can be removed by cyclic nucleotide binding. Different channel isoforms exhibit different sensitivity to cAMP modulation, in particular: $HCN2, HCN4 > HCN1 > HCN3$ [1]. Modulation of I_h properties occurs also in dependance of the intracellular levels of phosphoinositides like phosphatidylinositol-4,5-biphosphate (PIP_2). This class of molecules is able to shift the activation curve of Ih toward $\sim$ 20 mV more positive potentials. This regulatory mechanism operates in a manner independent from cyclic nucleotides and is equally effective on HCN 1,2,4 isoforms [115]. Regulation by phosphorilation is also reported for HCN channels, since in some preparations the cAMP modulation on I_h is completely abolished by applying protein kinase inhibitors. In a similar way, Ser/Thr inhibitors shift the activation curve toward more positive potentials, in particular PKA-mediated phosphorilation seems to preferentially happen [32].

The first HCN channel blocker known is the inorganic ion cesium, which is non-selective With respect to channel isoform and also acts as blocker for some potassium channels. More specific organic inhibitors are now available, developed mainly for their potential use as heart-rate reducing agents (see 1.2.4 for a detailed discussion). Among organic drugs, only the novel antiepilectic Lamotrigine shifts the activation curve of I_h in pyramidal neurons toward more positive potentials [85], thus acting as activator for HCN channels.

1.2.3 Physiological expression and role of HCN channels

HCN channels play a major role in the cardiac tissue, where they control rhythmicity in sinus-atrial node (SAN) pacemaker cells. In the SAN I_h is activated by membrane hyperpolarization leading to a progressive depolarization that, along with the contribution other calcium and sustained inward currents (I_{CaT}, I_{CaL}, I_{st}), takes the name of diastolic depolarization. In the cardiac tissue, channel isoforms mainly expressed are HCN4 and HCN2 (with the respective proportion of 80% to 20%). The other major function of I_h in cardiac tissue is the regulation of heart rate, operated by autonomous nervous system. Sympathetic stimulation of β-adrenergic receptors leads to an activation of I_h following to an increment in cAMP production. By contrast, Parasympathetic stimulation of muscarinic receptors induces a decrement of intracellular cAMP which negatively modulates I_h.

HCN channels are also expressed in dorsal root ganglion (DRG) neurons. In these cells HCN1 is the most abundant isoform, expressed by almost all the large- and medium-size neurons (A-type) at the level of their somatic membrane. HCN2 expression is lower, almost a half compared to HCN1 in every DRG neuron. HCN2 is mainly located on the membrane of large-body cells while intracellularly in small- and medium-body neurons, in the latter case it usually co-localizes with CGRP, the marker of nociceptive neurons [53]. HCN3 and HCN4 expression is much lower. Involvement of I_h in chronic neuropathic pain, a disease characterized by spontaneous pain, hyperalgesia and allodynia, is correlable to multiple aspects.

Ectopic potentials caused by some experimental models (sciatic nerve ligation, chronic constriction injury, DRG chronic compression) are reported to happen along with an up-regulation of I_h in these neurons, while application of the HCN channel blocker ZD-7288 significantly prevents ectopic discharges from injured neurones [12]. When discharges from injured neurons happen, adjacent nerves experience hyperexcitability, which results in an exaggerate perception of noxious stimuli as well as an increment in spontaneous activity. Few studies showed possible involvement of HCN channels as pro-nociceptive agents, since intraplantar injection of ZD-7288 alleviated thermal hyperalgesia in rats [17]. I_h involvement in regulating the axonal conduction and synaptic transmission in spinal dorsal horns is somewhat controversial and requires more clues (see [53]).

Within the CNS, HCN channels are widely expressed. HCN1 isoform is present in hippocampus, neocortex, cerebellar cortex and brainstem. HCN2 is expressed ubiquitously, but with particular abundance in brainstem nuclei and thalamus. HCN3 is present in retinal cones, only inside the olfactory bulb and in some hypothalamic nuclei its presence is medium to high. HCN4 is particularly expressed in thalamic nuclei and in the olfactory bulb, at level of mitral cell layer [73] [90] [79]. Near the resting potential HCN channels are usually open in these neurons and the resulting I_h contributes in setting and stabilizing the resting potential. Stabilization by constitutively open HCN channels acts in two distinct ways: by lowering the membrane resistance, therefore every input current induces a smaller change in membrane potential; and by actively counteracting to depolarizing or hyperpolarizing stimuli, acting as a slow "voltage clamp" mechanism able to suppress low-frequency fluctuations of the membrane potential. In dendrites of CA1 hippocampal neurons I_h influences the ampli-

tude and kinetic properties of excitatory post-synaptic potentials (EPSPs) [69] [70]. In the prefrontal cortex neurons it was shown that HCN co-localize with α_{2a} receptors for noradrenaline on dendritic spines, this made the authors suggest that decrements of cAMP produced by α_{2a} activation can modulate and reduce the open probability of HCN channels, augmenting the cellular susceptibility to synaptic inputs [104]. In cerebellar Purkinje cells I_h counteracts hyperpolarizing stimuli arriving to dendrites, stabilizing the membrane below the threshold for spontaneous spiking, this helps these neurons in maintaining an input-output relationship independent from previous activity's history. This, along with evidence that hcn1 knockout mice present deficits in learning motor tasks like rotarod or swimming, highlights an implication of HCN channels in motor learning [78].
Another major role for I_h in brain is to enable resonance in single neurons or modulate resonant behavior in neural networks. Resonance in a neuron is the property of responding preferentially to inputs of a defined frequency; to generate resonance a neuron needs to have properties of both low-pass and high-pass filter. The membrane properties account in every neuron for the low-pass filter. A current that opposes to changes in membrane potential it's needed to endow high-pass filter properties; and it's activation kinetic must be slower than the membrane time constant [49]. In this respect, I_h exhibits this feature and thus is a good candidate to generate high-pass filter properties. In fact several studies report I_h contribution in generating resonance in CNS neurons [103] [105] [47]. Inside known neural networks, I_h contribution is implied in generating theta oscillations [77] and also is an important player in generating γ-oscillations in hippocampus [30] [15], synchronized oscillations in the inferior olive [3] and subthreshold oscillations in enthorinal cortex [22] [39].

Peripheral expression of HCN was detected in the enteric nervous system, where all but HCN3 isoforms were detected [111]. An increment in I_h susceptibility to cesium blockade by AH neurons in distant colon was also observed in inflammed tissue [59]. HCN expression in non-neuronal cells is reported for pancreatic β-cells [26] and α-cell lines [113], in the latter case application of the HCN blocker ZD7288 enhanced glucagon secretion independently from glucose concentration.

1.2.4 HCN disruption insight on isoform relevance

Important insights on I_h-related disfunctions and pathologies comes from experiments of genetic deletion of hcn genes. HCN4 knockout mice die prematurely *in-utero* during day 9.5-11.5 of embryonic development, due to a deficiency in SAN [95]. Recording before the deadly period showed a cardiac I_f reduction by 85%, and an heart rate reduction by 40%. Most importantly these hearts are not sensitive to cAMP stimulation; this highlighted HCN4 as crucial in cyclic nucleotide modulation even in conditions where this isoform is not essential for heart beat generation. By creating Tamoxifen-inducible knockout mice for hcn4 it was possible to investigate the relative importante of HCN4 in adult cardiac tissue [44]. In these animals most of the sinoatrial I_f was eliminated, resulting in recurrent sinus pauses; on the other hand, heart rate is surprisingly still sensitive to sympathetic stimulation. Authors suggest that HCN4 may not be involved in physiological heart rate modulatory mechanisms, but could be instead a necessary component for maintaining a stable rhythmicity and to counteract parasympathetic heart rate decrements or transitions from stimulated to basal cardiac states (see fig. 1.9) [43].

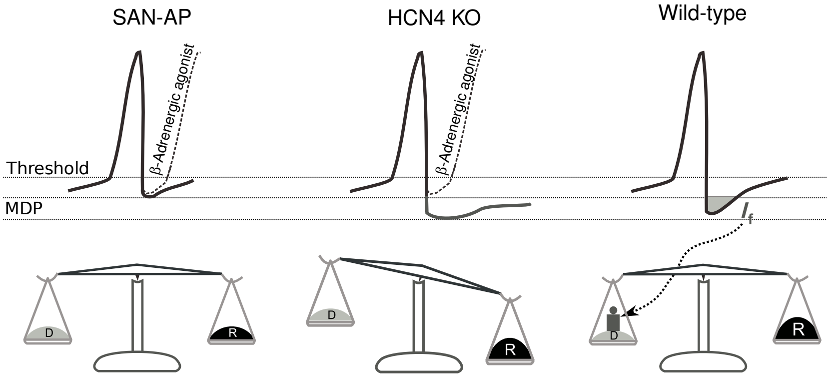

Figure 1.9: Hypothesis of HCN4 reserve-deposit in heart rate modulation. SAN-AP is the regular SAN action potential in wild type mice, whose length is shortened by noradrenergic stimulation. In HCN4 knockout noradrenergic stimulation still behaves as in wild type but following an increase in repolarizing currents (symbolized by R in the balance) I_f is required to join depolarizing currents (symbolized with D) in order to recover the balance. Figure adapted from [43]

Mice knockout for hcn2 are characterized by an hypoactive behavior and ataxic gait [61]. Electroencephalographic recordings and video analysis show occurrence of spike waves in correspondence to behavioral arrest, demonstrating that these mice suffer from absence epilepsy. Generation of spikes is probably related to increased excitability of thalamocortical neurones, since injection of positive currents into these neurons does not elicit single spike but results instead in burst firing. Calcium imaging in thalamic slices revealed oscillatory activity. These events are probably related to recovery of T-type calcium channels, normally inactivated at resting potential, by the induced hyperpolarization caused by lack of HCN2. At cardiac level these mice presents normal heart rate, with also a normal regulation of heart rate in response to motor exercise or administration of β-blockers. The only cardiac phenotype is a varying RR interval, resulting in sinus arrhythmia. Recordings from SAN cells showed a 25% reduction of I_f compared to wild type, resulting in a more hyperpolarized maximum diastolic potential. The mechanism hypothesized to cause sinus arrhythmia identifies HCN2 as useful in setting the diastolic potential toward more depolarized levels, a contribution that may become crucial in response to excessive hyperpolarization.

Deletion of hcn1 gene results in a viable phenotype, which presents deficit in learning motor tasks [78], especially the motor learning of fast movements (evaluated by rotarod and swimming tests). In these mutants spontaneous activity of Purkinje cells is not altered, demonstrating that HCN1 is not crucial for pacemaking in this neurones. However, in response to injection of hyperpolarizing currents, hcn1 knockout Purkinje cells display a profound hyperpolarization (normally counteracted by I_h) that strongly reduces firing. In addition, the Purkinje cell's firing independence on previous state is lost, and in knockout mice firing is much reduced if these cells experienced a previous silent state. The other major difference found in CNS resides at the level of hippocampal CA1 neurones, where deletion of hcn1 results in an enhancement of spatial learning and memory. This improvement affects both short- and long-term memory, and has an electrophysiological correlate in the enhancement of long-term potentiation (LTP) at the direct perforant path input to the more distal dendrite of CA1 neurones. No cardiac-specific phenotypes are reported for this mice.
Creation of hcn3 knockout mice has been made, but no clues on either cardiac nor brain phenotype are reported so far [68].

1.2.5 I_h current in the retinal tissue

The presence of a hyperpolarization-activated current was described in many of the retinal cells: photoreceptors, bipolar cells, amacrine and ganglion cells.

I_h is present in both rods and cones of amphibians, fish, molluscs and mammals; since the resting potential of these neurons is depolarized in dark conditions, I_h activates and plays a major role in shaping light response especially following a bright light. In rods, immunolabelling shows that the HCN1 isoform is particularly expressed in these neurons at the level of inner segment; while in the outer segment HCN are absent and thus no I_h may be detected recording from isolated outer segments [20]. This conductance in rods has the functional role to quicken the recovery of dark potential after a light response, providing a way to overcome the inherently slow speed of the rod phototransduction. In addition I_h filters the signal from noise before it reaches the synapse to bipolar cells [19] [18]. In cones the presence of HCN3 channels is reported at the level of terminal pedicles, while staining for HCN1 is present at the level of inner segment and somata [74].

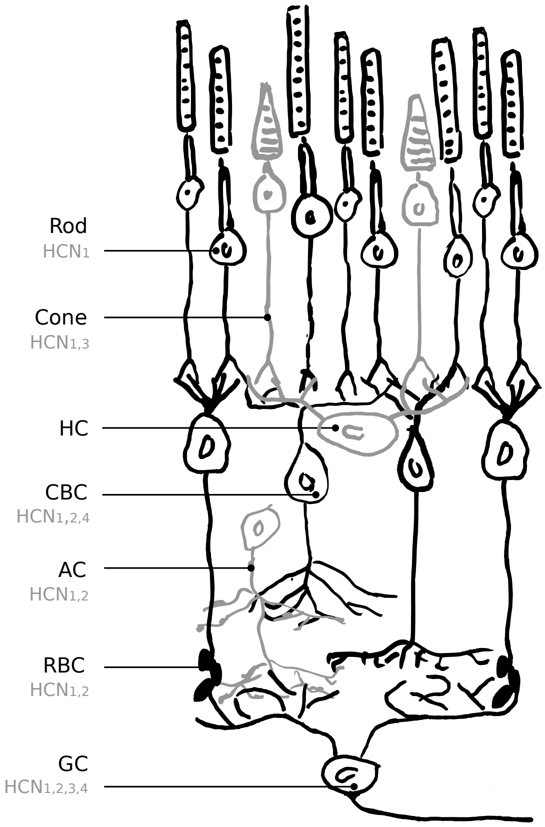

Figure 1.10: HCN distribution in retinal neurons. Rods [20], Cones [74], Cone Bipolar [50], Amacrine [57], Rod Bipolar [9] [56], Ganglion [74][57]

Retinal bipolar cells do also express HCN channels, in the mouse HCN1,2,4 isoforms were found to be expressed by cone bipolar cells [74][50][34]. In particular HCN4 are expressed by type3 bipolars, while type5 express both HCN1 and HCN4. Rod bipolar cells are reported to exhibit I_h in response to hyperpolarizing steps and this has been correlated with the expression of HCN2 channels in their axonic terminals [74]. Even if widely distributed among this neuronal class, some bipolar cells are also reported in literature to not exhibit I_h, in these neurons a time-independent potassium inward rectifier current is visible upon hyperpolarization [66]. Other papers report the presence of an hyperpolarization-activated current in bipolar cells also in lower-vertebrates [54] [13].

Amacrine cells of the mouse show I_h along with other potassium inward rectifiers in their dendritic compartment, as documented by recordings on horizontally sectioned retinae by Koizumi et al.[57]. Single-cell RT-PCR revealed that HCN1 and HCN2 are the only isoforms expressed by these cells. I_h stabilizes the membrane potential and has been proposed that the dendritic localization of HCN isolates functionally dendritic voltage changes evoked by synaptic inputs. This hypothesis, already formulated for hippocampal and cortical pyramidal neurons, has been validated even for smaller neurons like retinal amacrine cells by computational modelling of the cellular conductances, in starburst amacrine cells [57] [110].

Ganglion cells are also reported to exhibit I_h in both rat's [58] and goldfish's [100] preparation of isolated RGC. In this neuron I_h is suggested by the authors to play a role in both sustained and transient responses. I_h enables the RGC's membrane potential to sag in response to sustained light-induced hyperpolarization, and to recover in an accelerated manner at the termination of hyperpolarizing synaptic inputs. Additionally, since I_h reversal potential is more positive than the threshold of regenerative Na^+ and LVA Ca^{++} currents, it's activation may also increase the cell's excitability. Additional clues of HCN presence in this neuronal class come both from immunoistochemical studies, which showed HCN1 labelling among the ganglion cell layer[74], and from single cell RT-PCR where all of the four HCN isoform transcripts are found in the analyzed RGC[57].

1.2.6 HCN as therapeutic target for novel drugs

HCN channels represent an interesting target for the development of new drugs. Especially for their role in regulating the heart rate, HCN channel blockers are useful in treating arhythmic and ischemic pathologies. The key advantage of HCN blockers is the lack of side-effects typical of β-antagonists, like those on vascular or airway smooth muscle, since no HCN channels are present in these districts. Organic molecules that block cardiac I_f are:

- Alinidine (ST567), was discarded from clinical use since the lack of specificity, because it affected calcium and potassium currents along with causing a prolongation of the repolarization process.
- Falipamil (AQ-A39), Cilobradine (DK-AH 269), and Zatebradine (UL-FS 49) are compounds derived from the calcium antagonist Verapamil; all of them were able to block I_f current in a more specific manner than Alinidine, the blockade is use-dependant since requires the drug to act when the channel is open in order to induce blockade, unfortunately even these molecules had scarce clinical interest because of their side-effects especially on retinal I_h [91] [35].
- ZD-7288 was rejected from clinical use due to a proved interaction with I_h current present in substantia nigra [40] and hippocampal CA1 neurons [36] where it also interacts with LVA calcium currents [89].
- Ivabradine (S16257) is at the moment the only HCN blocker approved for clinical use [96], with indication for cases of angina pectoris where beta-blockers can not be used. The blockade exerted by Ivabradine on cardiac I_f develops in a use- and current-dependant manner, since blocking requires the channel to be in the open state and it is facilitated by depolarization, depending upon current flowing through the channel [8]. Visual disturbances were also reported for Ivabradine [7].

The most common among visual side-effects are stroboscopic, blurred vision and an increased occurrence of phosphenes, which are sensations of light not evoked by light stimuli (for a complete review see [10]). These side effects for Ivabradine are reported as dose dependent and generally disappear upon discontinuation of the treatment. The inhibition of retinal I_h by these organic drugs seems a possible reason for these side effects [18] [35] [67].

Another interesting field for developing new drugs involves the role of I_h in nociception, especially in chronic neuropathic pain. In this pathology HCN has been demonstrated to be involved in generation of spontaneous ectopic discharges from injured DRG neurons. Some papers reports that the HCN blocker ZD-7288 can prevent ectopic discharging, sensitization of nociceptors, axonal conduction and transmission in spinal dorsal horn. In this respect the different isoform distribution in dorsal root ganglia (where HCN1 is the predominant isoform) compared to the cardiac tissue (where HCN4 is the most abundant) provides a good incentive for development of isoform-specific HCN1 inhibitors.

An interesting possibility of drug development involves HCN as target for the treatment of epilepsy. hcn2 knockout mice exhibit a phenotype characterized by absence crysis [61]. In addition to this major evidence, some other studies evidenced possible HCN implication in temporal lobe epilepsy. Here a

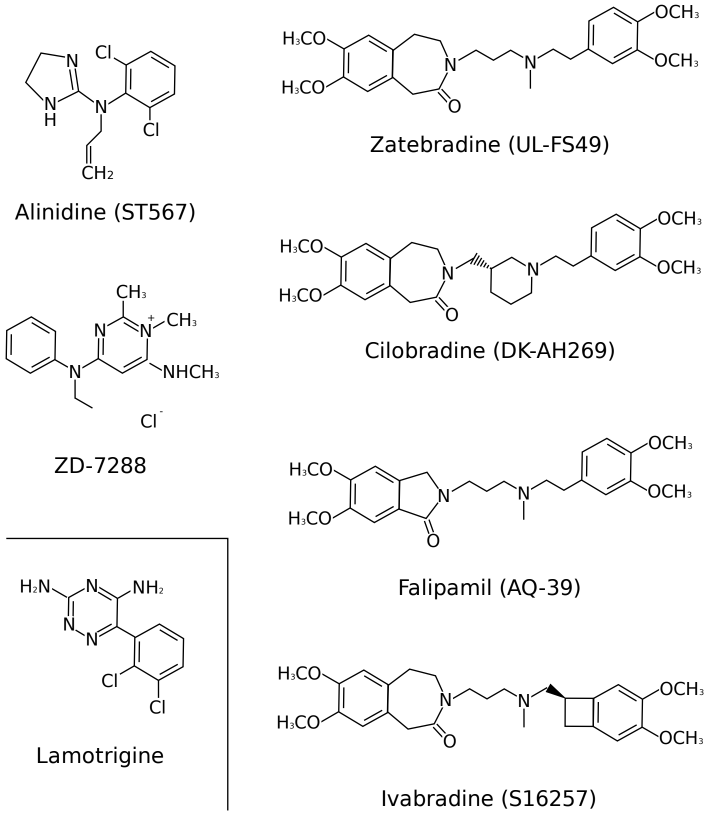

Alinidine (ST567)

ZD-7288

Lamotrigine

Zatebradine (UL-FS49)

Cilobradine (DK-AH269)

Falipamil (AQ-39)

Ivabradine (S16257)

Figure 1.11: Chemical structure of HCN-interacting organic molecules.

decreased I_h activity and channel expression was observed in a rat model of this pathology, conditioning the temporal coding and tuning of theta inputs in pyramidal cell dendrites [71] [86]. In support of this hypothesis, Lamotrigine, an antiepilectic drug characterized by unconventional structure, is able to shift the I_h activation range toward more positive potentials in rat's pyramidal neurons, thus controlling dendritic excitability and possibly being involved in epileptogenesis[85].

Chapter 2

Materials and Methods

> Foreman: *What'cha doin', Louie?*
> Louie: *I'm sawin' these planks, boss... got a bunch of 'em to do!*
> Foreman: *Umm, yeah... Louie*
> Foreman: *I can't tell for sure from this angle...*
> *but it looks like your saw's kinda dull.*
> Louie: *Eyes of a hawk, boss... I seen better edges on butter-knives!*
> Foreman: *Umm, yeah... so tell me, Louie*
> Foreman: *If you don't mind my askin'... why don'cha sharpen the saw, then?*
> Louie: *Oh, I can't do that now, boss... I'm too busy cuttin' these planks!*
>
> Sharpen the Saw: a Good Habit

2.1 Animals

All the experimental procedures involving animals were carried out according to the Italian and European guidelines for animal care (d.l. 116/92; 86/609/CE). Animals were maintained under a 12:12h light:dark cycle, with light period ranging from 7:00 to 19:00 regardless of national DST policy. Species and strains involved in this work include: Long evans rats (Charles River, Calco Italy), C56BL/6J mice (Charles River, Calco Italy), $B6; 129 - Hcn1^{tm2Kndl}/J$ mice (The Jackson Laboratories, Bar Harbor USA).

2.2 Patch Clamp

2.2.1 Slice preparation

Retinal slices were obtained from animals adapted for at least 2 hours in a completely dark room. All the procedures were carried out under dim red light. C57BL/6J mice were anesthetized with an intraperitoneal injection of avertin (Sigma-Aldrich, St.Louis MO, 15 mg/kg), their retinae explanted, then readily placed into cooled AMES medium (Sigma-Aldrich, St.Louis MO) equilibrated with a $95\%O_2 : 5\%O_2$ gas solution. Each retina was positioned vitreal side down over a filter paper (porosity 1.2 μm, Millipore, Billerica MA), the retinal surface protected by applying a thin layer of agarose (Type VII low gelling temperature, Sigma-Aldrich, St.Louis MO). Sections 250 μm thick were obtained with the aid of a manual tissue chopper (mod.600, The Vibratome Company, St.Louis MO). Once sectioned, retinal slices were transferred into the recording chamber where they were kept still by a thin mesh of nylon wire. The recording chamber, perfused constantly during the experimental session with oxygenated AMES medium, was placed under a microscope (DM-LFSA, Leica Microsystem, Wetzlar Germany) and the sample visualized under infrared illumination. Recordings were carried out at room temperature ($23°C$).

2.2.2 Pipettes

Glass pipettes used for perforated patch clamp were pulled with a P-97 (Sutter Instruments, Novato CA) and filled in the tip with a solution containing 94mM K_2SO_4, 20mM KCl, 10mM $NaCl$, 5 mM PIPES (all components from Sigma-Aldrich, St.Louis MO). The solution back-filling the pipette had the aforementioned composition with addition of 0.5mg/ml and 0.2mg/ml Amphotericin-B, the latter pre-dissolved into a 30mg/ml solution of DMSO (all components from Sigma-Aldrich, St.Louis MO). Final pipette resistance was in the range of 6-9 MΩ

2.2.3 Cell recording and identification

Pipettes were inserted into the tissue slice under visual control using a CCD video camera. A giga-seal was obtained by applying a gentle suction to the pipette. Recordings were performed using an Axopatch 1D amplifier, signals were low-pass filtered at 500Hz and digitized with a 5kHz sampling rate by a Digidata 1320a DAQ board; all the instrumentation was controlled via the PClamp 8 PC software (all from Axon Instruments, Foster City CA). Stray capacitance was minimized by placing a glass cover-slip treated with Sigmacote (Sigma-Andrich, St.Louis MO) in close proximity to the pipette tip. At the end of each recording the perforated seal membrane was disrupted, allowing the Lucifer Yellow dye to fill the cell cytoplasm for about 15-30 minutes; the cell morphology was then visualized using the epifluorescece module of the microscope. Focal plane images were serially acquired and merged together using a PC image manipulation software (Photoshop CS2, Adobe Systems Incorporated, San Jose CA). Rod bipolar cells were identified by the close proximity of their cell body to the outer plexiform layer as well as by their peculiar globular terminals present at the very inner portion of the inner plexiform layer. Unless otherwise stated, results are reported as mean value ± SD. Inhibition of HCN channels was obtained by application of ZD7288 (Tocris, Bristol UK).

2.2.4 Light stimulation

Flashes of light were generated by a LED light source (OD520, Optodiode Corp., Newbury Park CA), band-pass filtered (509-519 nm) and attenuated by using a neutral density optical filter (2log units). The light stimulation was placed beneath the recording chamber. Flash duration was in the range of 0.2-18ms, while flash energy was empirically adjusted to the sensitivity threshold of the recorded cell, so that occasional failures occurred on repetitive stimulation. Final light intensities were measured to be in the range of 0.3-1 $photons/\mu m^2$ at the bottom of the chamber using a radiometric probe Model 818-ST connected to an Optical Power Meter (both from Newport Corp., Irvine CA).

2.2.5 I_h characteristics evaluation

The perforated patch clamp technique allowed to record stable I_h current during the whole time of the experiment. The I_h activation function could not be reliably estimated by tail currents, since upon repolarization from very negative potentials, a transient inward current, possibly a calcium current, with inactivation kinetics overlapping the time course of I_h was present. Thus we fitted the family of current tracks during the hyperpolarizing step potentials with the equation (2.1):

$$\begin{aligned} i_{(t,v_{step})} &= G_{leak}(v_{step} - V_{leak}) + g_h(v_{step})(v_{step} - V_h) \\ &\quad -(g_h(v_{step}) - g_h(v_{hold}))(v_{step} - V_h)e^{\frac{-t}{\tau(v_{step})}} \end{aligned} \tag{2.1}$$

where: G_{leak} is the voltage and time independent leakage conductance; V_{leak} is the reversal potential of the leakage conductance; V_h is the reversal potential of I_h current, calculated using the Goldman-Hodgkin-Katz equation, assuming a Na^+/K^+ permeability ratio of 3:1 for HCN channels [108]; G_h is the maximum conductance of the I_h current; g_h is the steady-state I_h conductance at potential v, which is given by Boltzmann function (2.2):

$$g_{h(v)} = \frac{G_h}{1 + e^{\frac{v - v_{1/2}}{k_m}}} \tag{2.2}$$

where: $v_{1/2}$ is the half-activation potential for I_h and k_m is the inverse-slope factor All the unspecified parameter values were obtained as best fit on the experimental data, and also used to feed the simplified model explained below. Liquid junction potentials were calculated to be 10 mV using JPCalc (Axon Instruments, Foster City CA) and subtracted to each track.

2.2.6 Input impedance measurement

In order to establish the frequency-response relationship, we delivered in current-clamp mode a current stimulus which was sinusoidally modulated in time, also referred in the literature as a ZAP stimulus [87], whose frequency continuously and monotonically increased during the stimulation period, in a way defined by the equation (2.3):

$$f_{(t)} = f_{max}10^{\left(\frac{t-T}{T}\right)log\left(\frac{f_{max}}{f_{min}}\right)} \tag{2.3}$$

where: $f_{(t)}$ is the frequency value at time t; f_{max} and f_{min} are the maximum and minimum frequencies contained in the stimulus, respectively 0.1 and 30 Hz; T is the total duration of the stimulus, set to 50s. The current delivered to the cell was thus calculated with equation (2.4):

$$\begin{aligned} i_{(t)} &= I_0 \sin\left(2\pi \int_0^t f_{(t)}dt\right) \\ &= I_0 \sin\left(\frac{2\pi T}{ln\left(\frac{f_{max}}{f_{min}}\right)}\left(10^{\frac{t}{T}} - \frac{f_{min}}{f_{max}}\right)\right) \end{aligned} \tag{2.4}$$

The stimulus amplitude was calibrated so that the peak-to-peak amplitude of the voltage response remained within 10mV in the most of cases, this ensured both that responses were in a physiological range as during dim light stimulation, and that the system approached linearity (a requisite for harmonic analysis). Up to 9 sweeps were averaged in order to increase signal over noise ratio. The cell's complex impedance was calculated by the ratio of the voltage response FFT over the current stimulus FFT. The real modulus of the complex impedance (impedance profile) was plotted in the rage of 0.1 to 30 Hz. The analysis was performed with custom written routines in Axograph 4.9 (Axon Instruments, Foster City CA).

2.2.7 Input impedance modeling

By constructing a reduced cellular model we explored the role of I_h in providing frequency-tuning to the recorded neurones. The model consisted of the membrane capacitance, the ohmic leakage current, and I_h as the sole ionic active current. The outward current visible in experimental tracks (whose activation range did not overlap with the one of I_h) and the transient inactivating inward current were deliberately left out of the model. RBCs are well described by a single compartment model (as pointed out with direct experimental tests in [114]). Membrane capacitance was estimated for each cell way by fitting responses to small current steps with single exponential curve family. These steps were delivered in the narrow voltage range in which no active ionic currents were significantly activated (-70 to -75 mV). Leakage and I_h conductance parameters were estimated as described above. The simplified model can be linearized (in small-signals approximation), and its complex impedance derived as a function of frequency and membrane potential as reported in [48] and eq.18-19 in [46]. The simplified model thus allowed us to predict the cell behavior *a-priori*, since no free parameters are present in the model.

2.3 Immunohistochemistry

2.3.1 Slice preparation

Adult mice (age $\sim$ 2 months) were anesthetized with an i.p. injection of Avertine (15 mg/kg, Sigma-Aldrich). Eyes were enucleated and fixed by immersion in 4% paraformaldehyde for 15 min, eyecup was dissected and maintained in paraformaldehyde for 1 hour; washed in 0.1M phosphate-buffered saline (PBS, pH 7.4) and cryoprotected in scalar dilution (10, 20, 30%) of sucrose. Eyecups were then included in Tissue Tek Optimal Cutting Temperature (OCT) compound (Miles incorporated, Elkhart NL) and sectioned at $-20°C$ into a cryostat. Serial sections of $18\mu m$ in thickness were collected on glass slips coated with gelatin (Fluka Biochemika).

2.3.2 Immunoreaction

Primary antibodies were anti-Protein Kinase C (PKC, 1:200, Sigma-Aldrich); anti-HCN1, anti-HCN2, anti-Kv1.3 (1:200, Alomone, Jerusalem Israel), anti-HCN4 (1:100, Alomone), anti-mGluR6 (1:1000, Neuromics, Edina MN), anti-Bassoon (1:1000, Stressgen, San Diego CA). For all labelings, washes were 3x5 min in 0.1M PBS at room temperature; 1% bovine serum albumin (BSA) was used to block unspecific binding, while 0.3% Triton X100 was applied to induce membrane permeabilization for 30 min. The sections of the retina were incubated in diluted primary antibodies in the last solution, with 0.03% Triton X100 at $4°C$ overnight. Secondary antibodies were applied at room temperature for 2 hours. Secondary antibodies were anti-mouse or anti-rabbit conjugated with Alexa Fluor 488 (1:200) or with Alexa Fluor 568 (1:200, both from Molecular Probes). Separate control experiments were carried out for anti-HCN1,2 antibodies incubated with their respective immunizing peptide, in a ratio of 1:1. Retinal sections were visualized with a confocal microscope equipped with a krypton-argon laser (TCS-NT, Leica Microsystem, Wetzlar Germany), files were processed with an image manipulation software (Photoshop CS2, Adobe Systems Incorporated, San Jose CA).

2.4 Electroretinogram

2.4.1 Animal preparation

Animals were dark adapted overnight before the experimental session, both rats and mice were anesthetized with an i.p. injection of urethane (respectively 120mg/100g and 200mg/100g, Sigma-Aldrich). A single injection was sufficient to maintain the subject deeply anesthetized for the whole experimental session (3 to 4 hours), as verified by the absence of corneal reflexes. Pupils were dilated with drops of 1% tropicamide (rats) or 1% atropine (mouse) (both from Sigma-Aldrich), while constant body temperature of $\sim 37°C$ was maintained by an electric thermal blanket placed beneath the animal. A gold, ring-shaped recording electrode was placed over each cornea, a thin layer of methylcellulose (Lacrinorm, Farmigea Pisa) allowed the cornea to remain moist throughout the experiment. A gold-foil electrode placed in the mouth served as both reference and ground for the rat while, due to the smaller size, a needle electrode inserted in the rear portion of the neck was used for ground signalling in mice. ERG signals were amplified by a 1000x factor and filtered in the frequency range of 0.3 - 500 Hz by a PC board amplifier (LACE elettronica, Roma Italy), digitized at 12.8 kHz by a 16-bit DAQ board (model PCI-MIO-16E4) driven by a custom made LabView 6.1 software (both from National Instruments, Austin TX)

2.4.2 Drug delivery

HCN channel blocker Ivabradine (I.R.I.S., Paris France) was used for blocking HCN channels during in-vivo experiments.

In rats, acute administration was carried out using a catheter inserted into the jugular vein; while chronic drug delivery was achieved by implanting subcutaneous osmotic pumps (model 2ML4, Alzet, Cupertino CA), capable to deliver drug with a constant rate for a maximum time period of 4 weeks. Osmotic pumps were filled with a solution designed to deliver an initial drug dose of 13 mg/kg pro die. Animals were divided in 3 treatment groups: control group, receiving vehicle only; chronic group, undergoing 21 days of continuous treatment; recovery group, receiving the drug for 21 days followed by 7 days without treatment. At the end of the treatment period, osmotic systems were surgically removed from each subject. By weighting the residual content of the system and taking into account the animal's ponderal increment, we estimated that the systems delivered a average daily dose of 11.16 ± 0.32 mg/kg for the chronic group and 11.15 ± 0.24 mg/kg for the recovery group (values expressed as $mean \pm S.D.$, n=6). In order to implant the osmotic pumps, rats were kept under surgical anesthesia of 28mg/100g Avertine (Sigma-Aldrich). We performed a small incision in the skin between the scapulae, followed by a gentle spreading of the tissue around the incision point, which led to the creation of a subcutaneous pocket big enough to wrap the osmotic system. The cylindrical-shaped osmotic pump was then inserted with the flow moderator pointing to the opposite direction from the incision point; mechanical stability of the pump was ensured by binding it firmly near the backbone with surgical sterile suture. The skin incision was closed using wound clips.

2.4.3 Light stimulation

Light stimulation protocols were generated by a 16-bit PC DAQ interface (PCI-MIO-16E4, National Instruments, Austin TX), voltage-encoded signals were converted into light intensity variations by a device developed in our laboratory, described in [21]. Light stimuli were delivered into a Ganzfeld sphere of 30 cm in diameter, with internal surface coated with highly reflective white paint, in order to ensure an uniform illumination over the whole retinal surface.

For the flash stimulation protocol, an electronic flash unit (Sunpak B3600 DX , Tocad Ltd. Tokyo JP) delivered flashes of white light, whose energy decayed with a $\tau = 1.7$ ms and whose scotopic efficacy was estimated following [65]. The estimated retinal illuminance was 5.7×10^5 Φ (Photoisomerization per rod) per flash. The whole spectrum of light intensities were achieved by placing optical neutral density filters within the light path. For the sinusoidal stimulation protocol, light was generated by a LED source (OD520, Optodiode Corp., Newbury Park CA), band-pass filtered at 510 nm. The luminance was expressed as a function of time by the equation(2.5):

$$\begin{aligned} L_{(t)} &= L_0 \left(1 + m \cdot sin\left(\omega t\right)\right) \\ &= L_0 \left(1 + m \cdot sin\left(2\pi\nu t\right)\right) \end{aligned} \tag{2.5}$$

where: L_0 is the mean luminance, estimated to be ~ 40 ϕ; m is the contrast value, allowed to assume values from 0 to 1, a constant value of 0.85 was used during all the experiments; ν is the frequency of the generated sinusoid, varying from 0.3 Hz to 30 Hz within each trial.

Estimations of light intensity impinging on the rodent retina were carried out according to [64] using the equations (2.6) (2.7).

$$F_{(\lambda)} = \frac{I}{E_{photon}} = \frac{I}{h \cdot \frac{c}{\lambda}} \tag{2.6}$$

where: $F_{(\lambda)}$ is the photon density $[photons\ m^{-2}\ s^{-1}]$; I is the measured irradiance $[W\ m^{-2}]$; h is the Planck constant (6.6626×10^{-34} $J\ sec^{-1}$); c is the light's speed in a vacuum (2.99792×10^8 $m\ s^{-1}$) and λ is the wavelength of the light [m].

$$\frac{\Phi}{\Delta t} = F_{(\lambda)} \cdot \tau_{(\lambda)} \cdot a_{c(\lambda)} \cdot \frac{S_{pupil}}{S_{retina}} \tag{2.7}$$

where: $\frac{\Phi}{\Delta t}$ is the estimated photoisomerization per rod per second delivered to the retina; $F_{(\lambda)}$ is the photon density; $\tau_{(\lambda)}$ is the transmission of the pre-photoreceptor ocular media (estimated as 0.7 for both rats and mice); $a_{c(\lambda)}$ is the "end-on collecting area" of rod photoreceptors (1.3 μm^2 for rats, 0.87 μm^2 for mice); S_{pupil} is the area of the fully dilated pupil (7.1 μm^2 for rats, 3.2 μm^2 for mice); S_{retina} is the area of the retinal tissue (55 μm^2 for rats, 18 μm^2 for mice)

Chapter 3

Results

> *A process cannot be understood by stopping it.*
> *Understanding must move with the flow of the process,*
> *must join it and flow with it.*
>
> The First Law of Mentat

3.1 In vitro studies

3.1.1 Murine RBCs exhibit I_h

We explored rod bipolar cell properties by using the perforated patch-clamp technique. Neurons were identified by both their light response's polarity and their morphology, visible upon filling the cell with Lucifer Yellow dye at the end of the experiment (fig. 3.1).

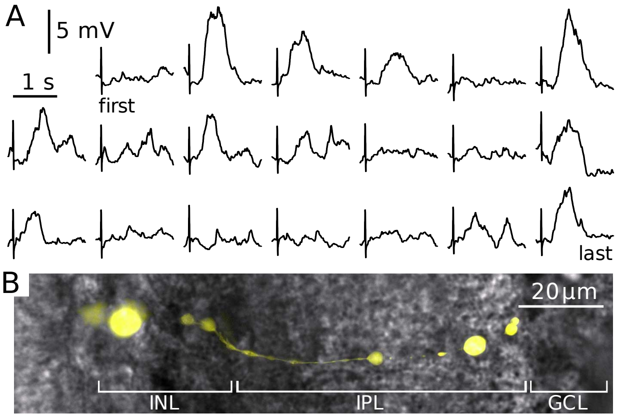

Figure 3.1: Functional and morphological properties useful for the identification of retinal RBCs. **A**: Light responses to weak, brief flash light stimuli (duration = 6 ms, interflash delay = 4 s). **B**: Staining of a RBC with Lucifer yellow after a recording session.

On average, recorded RBCs showed a resting membrane potential in dark-adapted conditions of $-74 \pm 4.7mV$, an input resistance of $3.2 \pm 1.0M\Omega$ and a membrane capacity of $25.4 \pm 6.7pF$. While recording the cell in Voltage-Clamp mode, delivery of hyperpolarizing voltage steps resulted in the activation of a slow, non-inactivating inward current whose activation constant shows time- and voltage-dependence, reaching its maximal value of $443 \pm 102ms$ in correspondence of half-activation potential (fig. 3.2 A). The following characteristics were peculiar of this current in our experiments (n=25): $G_h = 0.163 \pm 0.076nS$, $G_{leak} = 0.338 \pm 0.170nS$, $K_m = 6.3 \pm 0.7mV$, $V_{1/2} = -91.4 \pm 4.1mV$. At the end of the hyperpolarizing step, membrane potential was brought back to -60 or -75 mV in order to elicit tail currents; unfortunately in many of the recorded cells another current was superimposed to I_h deactivation. This additional current, visible upon repolarization from steps more negative than -90/-100 mV and unaffected by the application of HCN channel inhibitors, showed similar features to the current carried by T-type Calcium channel (already described in rat bipolar cells by [50], [41], [82]).

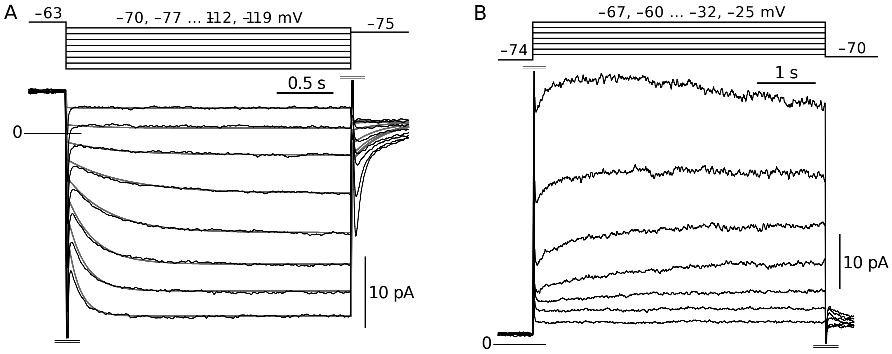

Figure 3.2: Voltage-Clamp protocols applied to the a representative RBC. **A**: Black trace, cellular response to hyperpolarizing steps; The gray trace is current response predicted by the simplified model. **B**: Cellular response to depolarizing voltage steps.

In response to depolarizing stimuli (fig. 3.2 B) two currents are visible: the first is an outward current, active from -70/-60 mV, with a slower kinetic than I_h and which does not exhibit inactivation, similarly to the I_{kx} present in rods [19],[4]. The second outward current, active from -50/-40 mV, readily activates and slowly inactivates, reaching amplitudes of hundreds pA when steps depolarized the cell to more than 0 mV.

The putative I_h current was confirmed by blocking it with the selective HCN blocker ZD7288 (fig. 3.3); we applied the drug into the perfusion circuit at concentration of 1 to 5 μM, it took from 10 to 25 minutes to almost completely abolish I_h, while tail currents were almost unaffected (stars in fig. 3.3 inset).

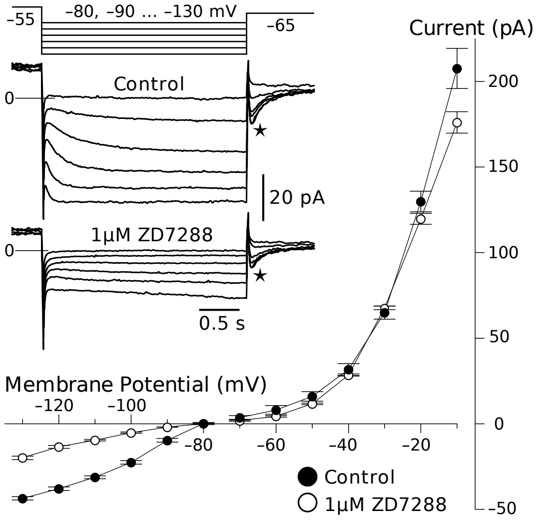

Figure 3.3: Voltage to current relationship before (filled circles) and after (open circles) application of the HCN channel blocker ZD7288. Note how the effect of the drug is present mainly for voltages lower than -80mV. **Inset**: Application of ZD7288 1 μM almost completely abolished the I_h current evoked by hyperpolarizing voltage steps.

3.1.2 Voltage-dependent impedance profile

The functional role if I_h was investigated by means of current-clamp recordings. By delivering a current step to the clamped cell, I_h presence becomes visible as a sag in the voltage response (fig. 3.4 A). This neuronal class does not produce spikes but instead responds to the signal arriving from photoreceptors with graded voltage changes. Cell properties were investigated by delivering small current stimuli sinusoidally modulated in time, with a frequency ranging from 0.1 to 30 Hz (fig. 3.4 B). Membrane potential of RBC is modulated in a sinusoidal way in response to this ZAP stimulus. The amplitude of the response becomes attenuated as the stimulus frequency increases. When the same stimulus was delivered in the range of I_h activation, the cellular response changes showing a resonance peak at intermediate frequencies. This behavior becomes more evident when the membrane potential is further hyperpolarized and I_h more activated.

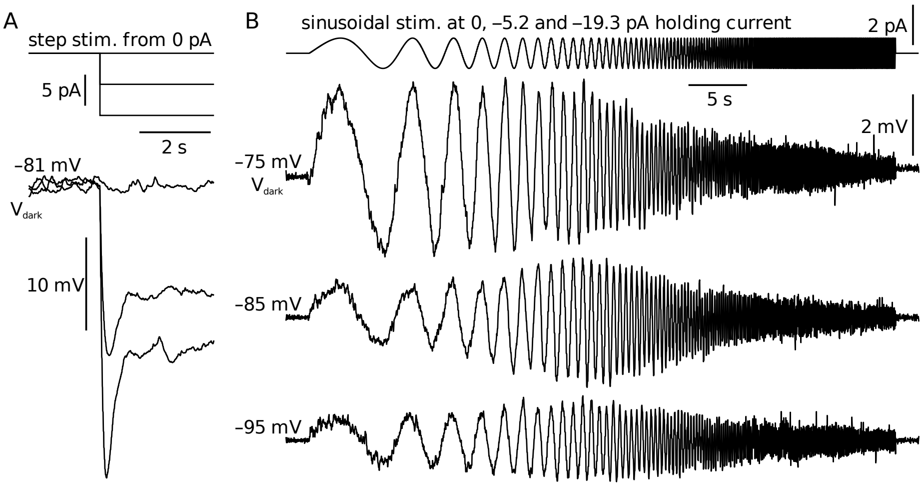

Figure 3.4: Current-clamp responses to voltage modulation in the range of I_h activation. **A**: Delivery of an hyperpolarizing current step highlights I_h's negative feedback role, visible as a sag in voltage tracks. **B**: Responses to a sinusoidally modulated current stimulus (highest track) at different holding potentials. Lower frequency sinusoids were more attenuated as the membrane potential becomes more negative and I_h current becomes consequently more active.

By calculating the system's complex impedance we analyzed the cellular properties in the frequency domain (see 2.2.6). RBCs shows a band-pass profile which is depends from voltage, and can be quantified by the band-pass index, defined as the ratio between the peak value of impedance modulus and the value recorded for the lowest frequency (0.1 Hz in this case). The band-pass behavior is present at two distinct voltage ranges: the first for membrane potentials more negative than -75 mV, corresponds to the range of I_h activation; the second for potentials more positive than -70 mV, clearly out of the range of influence of I_h, where the I_{kx}-like current is present (fig. 3.5 a-f). Another interesting feature is that in contrast to the relative influence of voltage on the band-pass index, the frequency at which the impedance reaches its maximal value remains around 1 Hz for the whole voltage range where I_h is active (fig. 3.5 g). We

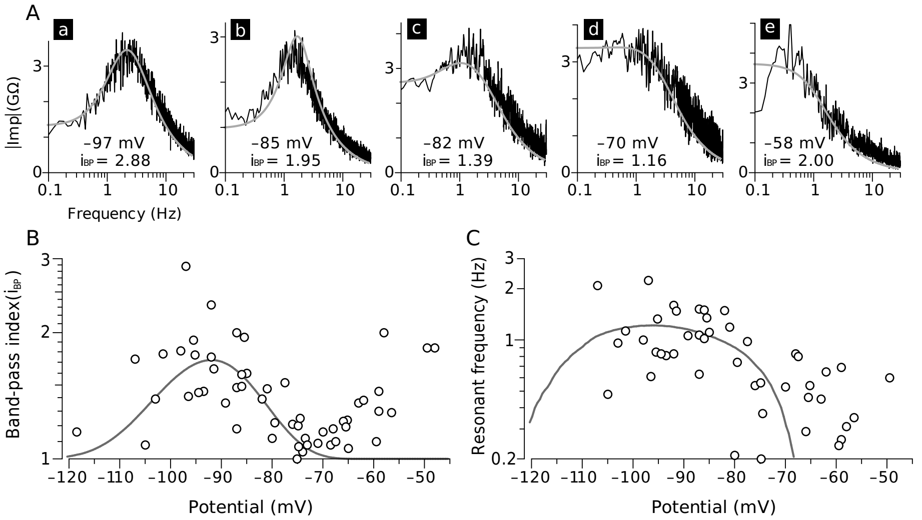

Figure 3.5: Input impedance analysis reveals band-pass filtering of input signals by RBC. **a-e**: Representative impedance profiles obtained by delivering sinusoidal stimulus at different membrane voltages; experimental values in black; simplified model prediction in red. **f**: Amount of band-pass behavior with respect to membrane voltage; experimental values as circles, prediction of the simplified model for the mean in gray. **g**: Voltage dependence of resonant frequency; experimental values as circles, predicted values by the model in gray.

propose a simplified model for each recorded neurone, assuming I_h as the only active conductance (see 2.2.7 in methods for details). The goal of the model was to understand if the presence of I_h was sufficient to explain the impedance profile distinctive of these cells. This model was fed with experimental values of membrane capacitance, leakage current and I_h properties, then asked to predict *a-priori* the impedance profile of the cell. For every recorded neurones, the model was able to predict with good approximation the experimental data, confirming that in the voltage range of I_h activation, this current is sufficient to explain the impedance profile of the cell (fig. 3.5 a-e gray traces). At the same time, the simplified model was able to predict the voltage dependace of band-pass index and resonant frequency (fig. 3.5 B,C gray traces), showing how the band-pass behavior reaches its maximum in correspondence to I_h's half-activation potential.

A direct confirmation that the band-pass behavior is associated to the HCN gating was obtained by application of the HCN channel blocker ZD7288. The sinusoidal stimulation was repeated in control condition and after effective blockade of I_h by ZD7288; Under these conditions, when I_h is no more active in the cell, the impedance profile switches from a band-pass to a low-pass mode (black traces in fig. 3.6). For the same cells we also predicted the effect of blocking the I_h current by setting the I_h conductance inside the model to zero (red traces in fig. 3.6).

3.1.3 Influence of I_h on light responses

How may the presence of I_h affect the cell's response to physiological input evoked by light stimulation?
In order to answer this question, we firstly recorded in voltage clamped the current evoked by dim light flashes (estimated intensity: 1.5 $photons/\mu m^2$ or 3 times the intensity able to induce a 50% of failures in the response), maintaining the cell clamped at -85mV, a voltage where a strong band-pass behavior is present ($I_{bp} = 1.59$). The recorded synaptic current was then fed into the model in order to predict the voltage response of the same cell to this stimulus. The resulting prediction is remarkably similar to the experimental recording performed in the same cell (fig. 3.7 A), showing how for small signals the rod bipolar cell response is the same no matter where the stimulus is applied, to dendrites or to the cellular body. Since on pilot experiments we noted that application of HCN blockers also affects synaptic currents, the influence of blocking I_h in RBC was tested using the simplified model. Upon inhibition of I_h in the model an increment in amplitude and duration for flash responses are visible (fig. 3.7 B1). I_h does not simply perform a size scaling of the signal, but also changes the time scale. This can be appreciated by comparing the normalized responses before and after HCN inhibition (fig. 3.7 B2). This property may narrow the integration time useful for summating two nearly-coincident stimuli incoming to the same RBC. This possibility was also tested using our simplified model. The results are illustrated in 3.7 C, where two identical synaptical stimuli were applied subsequently with increasing delay. It is visible how the the second flash's amplitude depends upon the delay between the two stimuli. When I_h is present, the amount of time useful for temporal summation of the two stimuli greatly diminish, and for times beyond 300 ms the second flash response becomes also attenuated. Instead, when if I_h is not present, temporal summation happens until a delay of 600 ms.

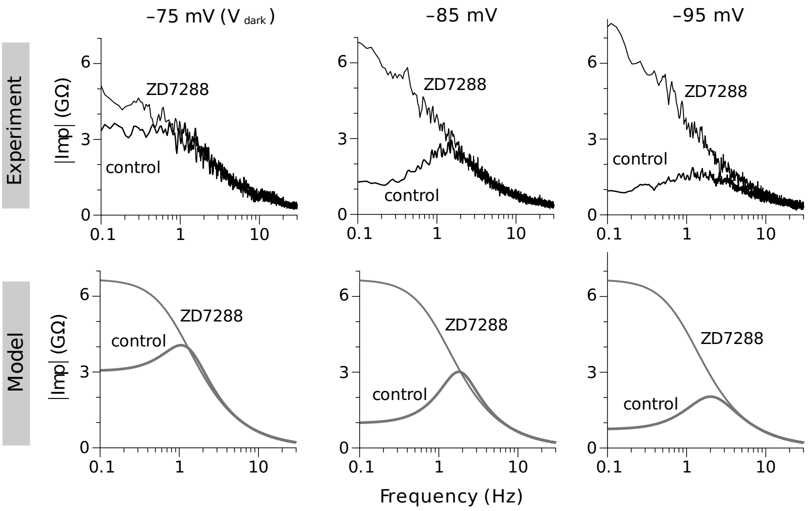

Figure 3.6: Input impedance profiles in control condition and after application of 1 μM of the HCN channel blocker ZD7288. Experimental impedance performed at -75, -85, -95 mV; before and after application of the blocker in black on upper panels. Predicted models for the same cell in gray on lower panels.

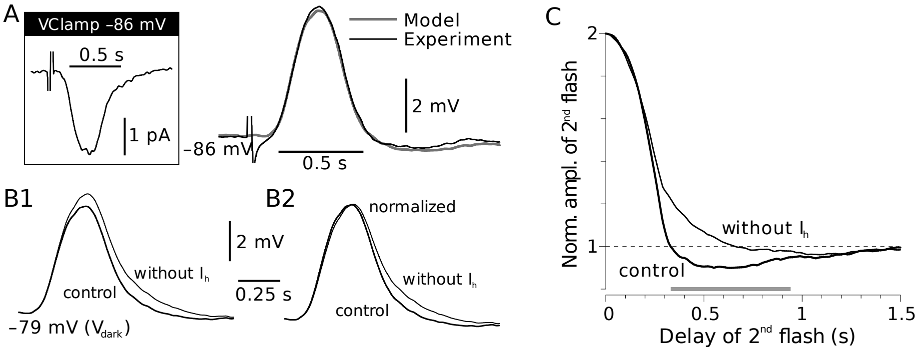

Figure 3.7: Presence of I_h quickens the cellular response to a single flash and narrows the time interval useful for detecting event coincidence. **A**: Post-synaptic current recorded in response to a weak flash (3 times the threshold intensity) recorded in voltage-clamp on the left, and in current clamp on the right, predicted response of the model in gray. **B**: Post-synaptic potentials evoked in presence or absence of I_h, absolute values in B1, normalized traces in B2. **C**: Response to a second flash delivered at increasing delay from an analogous first stimulus in presence or without I_h; values expressed as relative to first flash's response.

3.1.4 HCN distribution in the murine retina

We examined HCN channel distribution in the murine retina in order to understand which HCN isoforms may drive the I_h current recorded from RBCs. Staining of retinal section against HCN1 revealed this isoform is widely expressed in the retina, its labeling is visible in the inner segment and cellular body of rods, as well in both internal and external plexiform layers. In addition, individual cells stained by anti-HCN1 are present in the inner nuclear layer (see fig. 3.8). HCN2 staining shows a quite restricted localization: the major visible staining occurs at the level of OPL, where it takes the form of discrete spots; it is also present a weaker staining in correspondence to the IPL. HCN3 distribution in the retina was not evaluated in this study, since the only commercially available antibody revealed as ineffective for the use in immunohistochemistry. Anyway it is already reported in literature [74] that immunolabeling against HCN3 is localized at the level of cone pedicles and, in a weaker manner, at the level of IPL. Staining against HCN4 showed a localization at level of INL, on some bipolar cell bodies, dendrites and axons. The axon terminals of these cells end on layer two of IPL and identify these cells as OFF cone bipolar cells (see [106]). It should be noted, however, that anti-HCN4 antibody also stains some cell bodies of ganglion cells (also confirmed by [80]).

The relative localization of HCN2 at the level of OPL was analyzed in detail by using double staining with known pre-post synaptic markers. HCN2/PKCα labeling at OPL level shows how HCN2 clusters distribute in close proximity to RBCs' dendritic tips. We compared this distribution with the one of metabotropic glutamate receptor mGluR6 and the one of inward-rectifier potassium channel Kv1.3, since both these proteins are known to be located postsynaptically onto RBC dendritic tips. HCN2 distribution is remarkably similar to that of both them. In order to confirm whether HCN2 is pre- or post-synaptic to the rod-RBC synapse we also performed double-labeling of HCN2 and the presynaptic protein bassoon, a cytoskeleton component in rods' synaptic ribbons. This double labeling shows HCN2 as juxtaposed to the synaptic ribbon, without any evident presence of co-localization with bassoon, exactly like how happens for the post-synaptic mGluR6 and Kv1.3 proteins. This channel isoform is thus a good candidate to be, at least in part, a contributor to the current I_h recorded from RBCs.

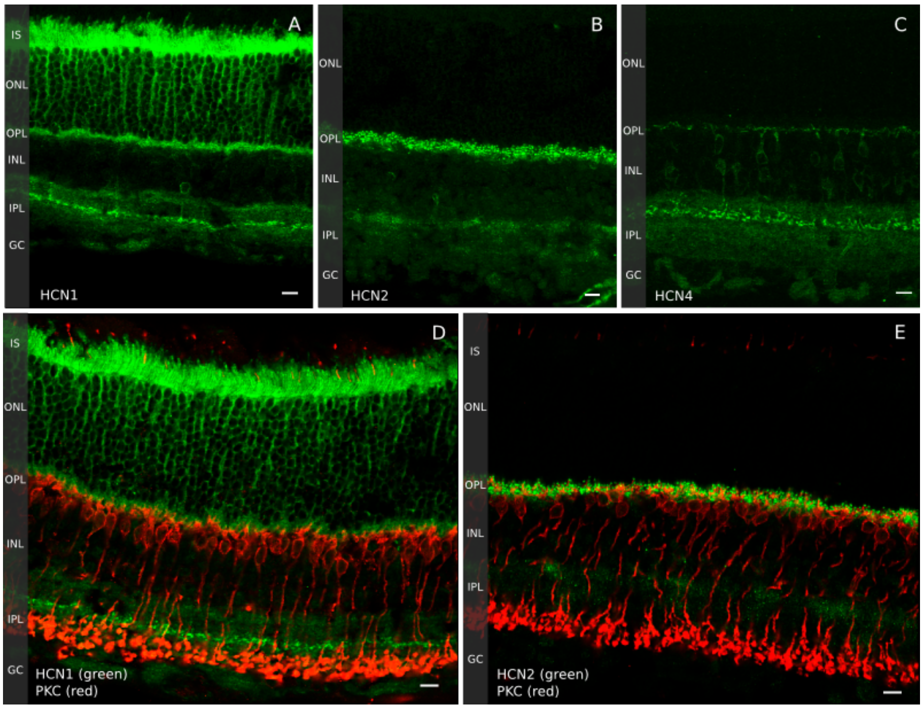

Figure 3.8: Confocal micrographs of retinal frozen sections, stained with antibodies against HCN channel isoforms. **A**: HCN1 subtype distribution: Staining is present at the level of rod inner segments (IS), outer nuclear layer (ONL), outer and inner plexiform layer (respectively OPL and IPL).**B**: HCN2 subtype localizes mainly at the level of OPL, with also a weaker signal present in the outer portion of IPL.**C**: HCN4 subtype localizes at the level of OPL; in some bipolar cells, in IPL with more intense band and with a lesser extent on GC. **D**: Double staining with anti-HCN1 (green) and anti-PKCα (red) shows no apparent zone of co-localization of the two labelings at the level of RBCs. **E**: Double staining with anti-HCN2 (green) and anti-PKCα (red) shows an intriguing proximity of the outer HCN2 labelling with RBCs dendrites. Scale bars 10 μm.

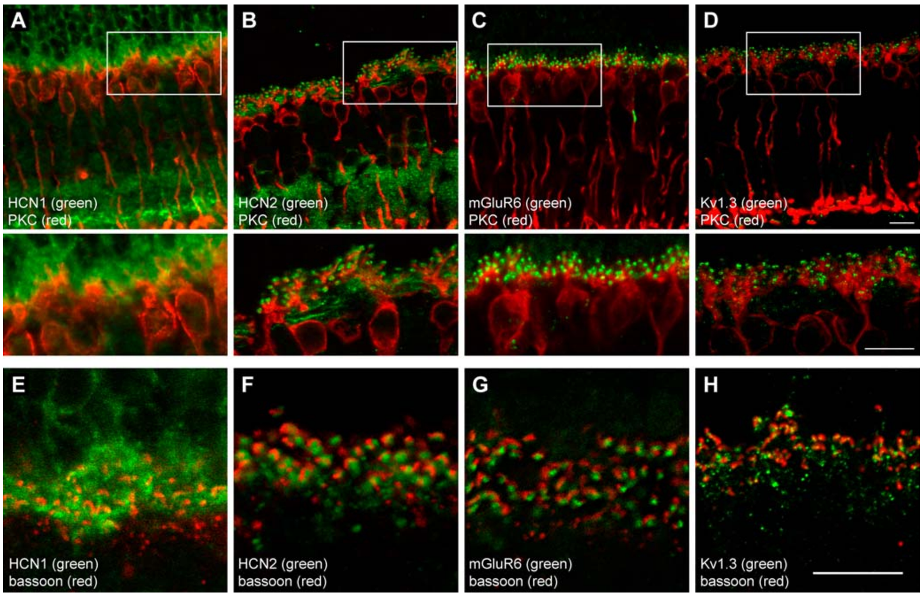

Figure 3.9: Double labelings with rod pre- and post-synaptic proteins, with focus on the OPL layer.**A**: HCN1/PKCα shows a diffuse localization of HCN1(green) in the OPL without co-localization with RBC dendrites.**B**: HCN2/PKCα labeling highlights HCN2 (green) positioning on RBCs' dendritic tips.**C**: Metabotropic glutamate receptor mGluR6/PKCα, this postsynaptic receptor (green) on RBC distributes on dendritic tips in similarity to what seen for HCN2.**D**: Potassium channel Kv1.3/PKCα, this channel (green) known to be placed on RBC dendrites also shows a similar distribution to HCN2.**E**: Staining against HCN1 (green) and the pre-synaptic protein Bassoon (red). **F**: HCN2/Bassoon shows HCN2 labeling (green) aligned to "C" shaped synaptic ribbons delimited by Bassoon (red), in a similar way to mGluR6 (green in **G**) and Kv1.3 (green in **H**). Scale bars 10 μm.

3.2 In vivo studies

3.2.1 Acute I_h inhibition in rats

What is the in-vivo influence of I_h on retinal processing? This issue was investigated by recording ERG in both rats and mice in control conditions and in the presence of HCN blockers. In order to efficiently and safely block HCN channels during in-vivo recording, Ivabradine was chosen as blocker because of its specificity [18] and low toxicity [27]. We tested the ERG response to both brief flashes and sinusoidally modulated light stimulation resorting in rats to two distinct dosing approaches: acute and prolonged administration.

For the acute study, a single dose of blocker was injected into the jugular vein, heart rate was monitored as an indicator of systemic drug efficacy. Within a few minutes the drug induced a consistent reduction of heart rate which slowly recovered after several hours. Acute HCN inhibition induced on flash ERG only a slight increment in amplitude (measured as b-wave amplitude in fig. 3.10 A), while at the same time the flash sensitivity at every tested time is not affected by the acute treatment (fig. 3.10 B). By looking at single ERG traces (a representative example in fig. 3.11), the late phase of Flash response tends to be prolonged when I_h is inhibited with respect to control. Especially at lower light intensities, a reproducible rebound oscillation happens delaying the time required for the response to extinguish (upper panels in fig. 3.11).

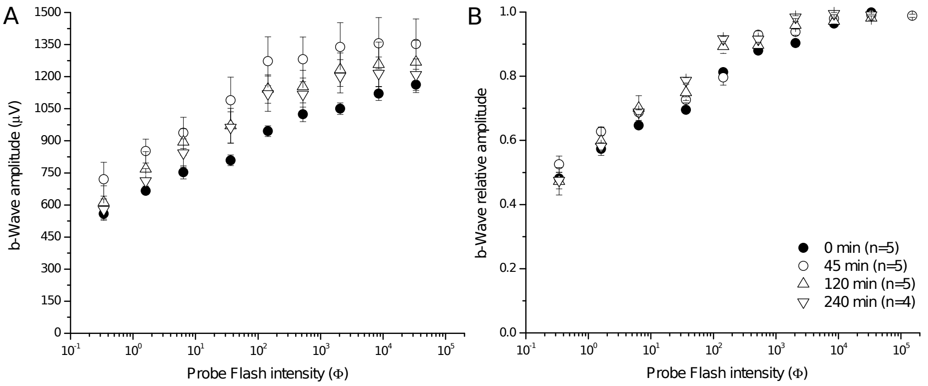

Figure 3.10: ERG's b-wave amplitude measurements in control condition (filled circles) and at progressive times from i.v. injection of Ivabradine 12 mg/kg. **A**: Absolute b-wave amplitudes (mean±SEM) **B**: Relative b-wave amplitudes (mean±SEM), each track normalized to its maximal value; shows that no alteration in light sensitivity happens as a consequence of I_h inhibition for the tested luminance.

The temporal resolution was evaluated by using a sinusoidal stimulation protocol (see 2.4.3 in methods), this is done by analyzing the first harmonic of the ERG response to a light stimulus sinusoidally modulated over a weak light background. In control conditions rat's ERG response has the characteristic shape of a band-pass filter, with the maximal response to stimuli of frequency around 1 Hz (filled circles in fig. 3.12). After the injection of 12 mg/kg, the response profile changes from the band- to low-pass mode. In particular frequencies between 1 and 10 Hz are greatly attenuated, with a maximal reduction

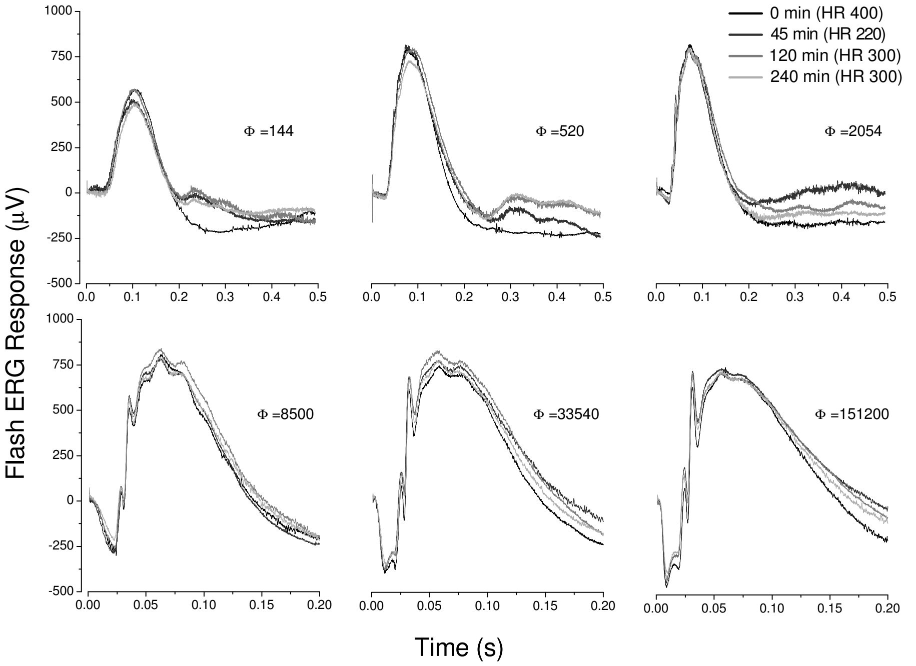

Figure 3.11: Representative example of Flash ERG responses after an i.v. dose of Ivabradine 12 mg/kg, black trace represents control condition, traces are average of 3-5 sweeps. Upper panels: note at lower light intensities an oscillation is present in the late phase of erg response. Lower panels: no evident alteration on ERG amplitude, only a delayed repolarization is sometimes visible.

around 3 Hz. However the profile does not switch to a simple low-pass filter like what already seen on RBCs (see fig. 3.6). The dose dependence of this effect points to a specific consequence of HCN inhibition (fig. 3.12 B).

A convenient parameter to quantify this profile change is the ratio (R_{3Hz} / $R_{0.3Hz}$) between the response occurring at 3Hz, the frequency most affected by the inhibition, and the response at 0.3 Hz, the lowest stimulus frequency whose response may be reliably measured with our instrumentation. By plotting this parameter superimposed to heart rate frequency (fig 3.13) it is possible to compare the effect on cardiac HCN with that on retinal HCN. In vehicle injected subjects neither the effect on heart rate nor that on ERG change significantly after injection. Upon injection of increasing doses of HCN blocker (3,6,12 mg/Kg), the effect on frequency profile (histograms in fig 3.13) increases progressively in a dose-dependent manner, without any sign of consistent recovery in the analyzed time-span of 3 hours from the injection moment. In a similar way, the effect on heart rate is dose dependent (filled circles in fig. 3.13), significant for every time after injection in all tested dosages (two-way ANOVA, followed by Tuckey multiple comparison tests). The effect on heart rate develops and reaches its maximum just after the injection, with a slow but detectable recovery during the following 3 hours; while the effect on ERG develops with a slower pace, and reaches its maximum only 90 minutes after the injection, without recovery after 3 hours.

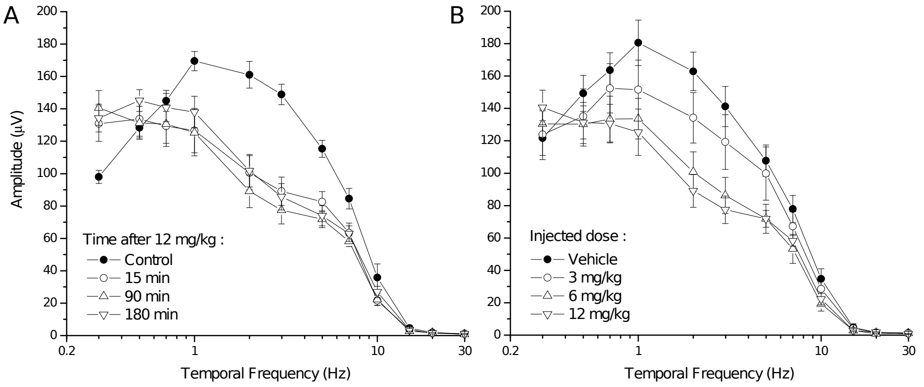

Figure 3.12: Frequency-response profile changes from a band-pass to a low-pass-like shape. **A**: Profiles acquired in control condition (filled circles) and at progressive times from a 12 mg/kg Ivabradine injection (mean±SEM, n=6). **B**: Profiles recorded after 90 minutes from an increasing i.v. dose of Ivabradine. Tested doses were 0,3,6,12 mg/kg (mean±SEM, respectively n=5,4,5,6).

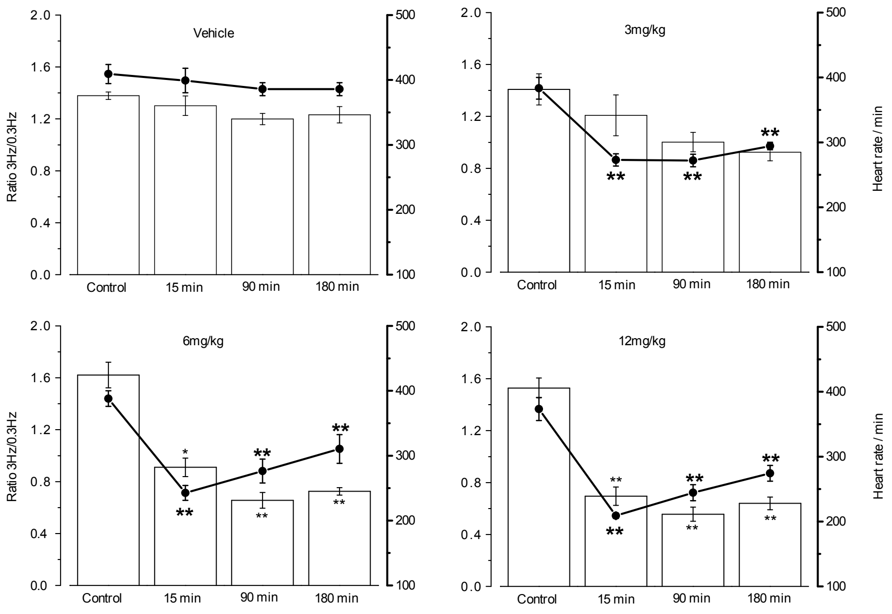

Figure 3.13: Effect of acute HCN inhibition on heart rate (filled circles, thicker asterisks) and on response to sinusoidal stimulation (mean ± SEM, n=6), the latter expressed as ratio between the response at 3Hz and 0.3Hz (histograms, light asterisks). Effect on heart rate develops just after injection with a slow but appreciable recovery. Action on ERG develops later than bradicardia with no recovery observed after 3 hours (* means $p < 0.05$, ** $p < 0.01$ Tuckey multiple comparison after 2-way ANOVA).

3.2.2 Prolonged I_h inhibition in rats

In addition to acute Ivabradine delivery we also analyzed the effect of a prolonged treatment during a temporal window of weeks. Prolonged, continuous dosing was obtained by means of subcutaneously implanted osmotic pumps loaded with a saline solution of the drug (see 2.4.2 in methods). This allowed a constant release of the inhibitor for the whole treatment period. Three experimental groups were defined: a control group which received only vehicle, a chronic group receiving an initial daily dose of 11 mg/kg for 3 weeks, and a recovery group receiving a 3-weeks treatment followed by one week without treatment. At the end of each treatment period, ERG in response to flash and sinusoidal stimuli was recorded. Flash protocol was expanded to comprise a full spectrum of light intensities since following a long-term treatment, flash sensitivity changes are more likely to happen. Anyway, by looking at flash ERG responses (fig 3.14) the b-wave amplitude does not change following chronic administration nor does the relative flash sensitivity undergo visible changes.

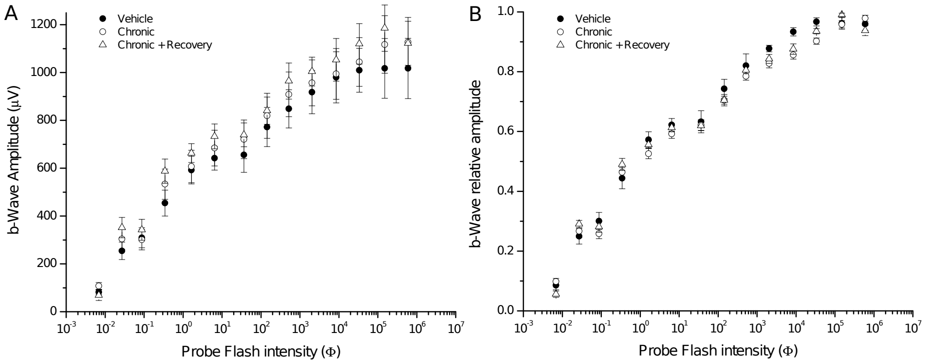

Figure 3.14: ERG's b-wave amplitude measurements during chronic administration of vehicle (control group, filled circles), 21 days of HCN channel blocker (chronic group, open circles, average dose 11.16 ± 0.32 mg/kg Ivabradine), and 21 days of HCN blocker plus one week of treatment interruption (recovery group, open triangles, average dose 11.15 ± 0.24 mg/kg Ivabradine). **A**: Absolute b-wave amplitudes (mean±SEM, n=6) **B**: Relative b-wave amplitudes (mean±SEM, n=6), each track was normalized to its maximal value. No alteration in b-wave amplitudes or light sensitivity happens as a consequence of I_h inhibition for every tested luminance.

Frequency-response profiles after prolonged HCN blockade closely resemble the effect of single i.v. injection (fig.3.15 A), with a substantial loss of frequency preference. This effect almost completely reversed to control value one week after Ivabradine dosing interruption. By plotting the ratio $R_{3Hz}/R_{0.3Hz}$ superimposed to heart rate (fig.3.15 B) it's evident how both these parameters undergo a substantial decrease following chronic I_h inhibition and return to control values after recovery period.

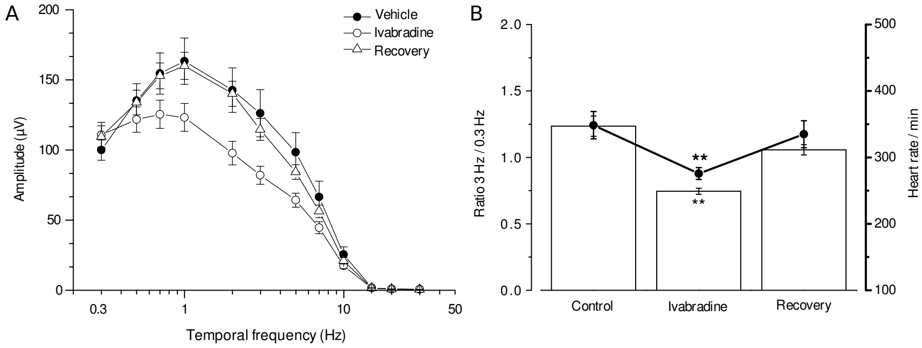

Figure 3.15: Effect of chronic administration on temporal properties and heart rate (values expressed as mean±SEM, n=6) **A**: Frequency-response profile in vehicle-treated group (filled circles), HCN blocker group (open circles) and recovery group (open triangles) shows an inhibition effect similar to what seen during acute administration **B**: Ratio $R_{3Hz}/R_{0.3Hz}$ (histograms, light asterisks) and heart rate (filled circles, thick asterisks) shows a significant decrease after treatment that is reverted to control values after one week drug-free (* means $p < 0.05$, ** $p < 0.01$ Tuckey multiple comparison after 2-way ANOVA).

3.2.3 hcn1 knockout mice

What is the relative influence on temporal properties of HCN1 (mainly expressed in rods) with respect to the other isoforms?

Since the unavailability of HCN channel blocker molecules selective for a specific channel isoform, we evaluated retinal performance on a murine animal model knockout for the hcn1 gene (hcn1-ko, see 2.1 in methods). Since rods in the mouse represents the majority of photoreceptors ($\sim$ 97%), the recorded ERG signal is expected to be particularly susceptible to changes happening on the rod pathway. Rods of hcn1 knockout mice do not exhibit I_h in response to hyperpolarizing steps (fig.3.16 B), while in control wild type mice, a visible hcn1-driven I_h is activated in response to the same protocol (fig.3.16 A).

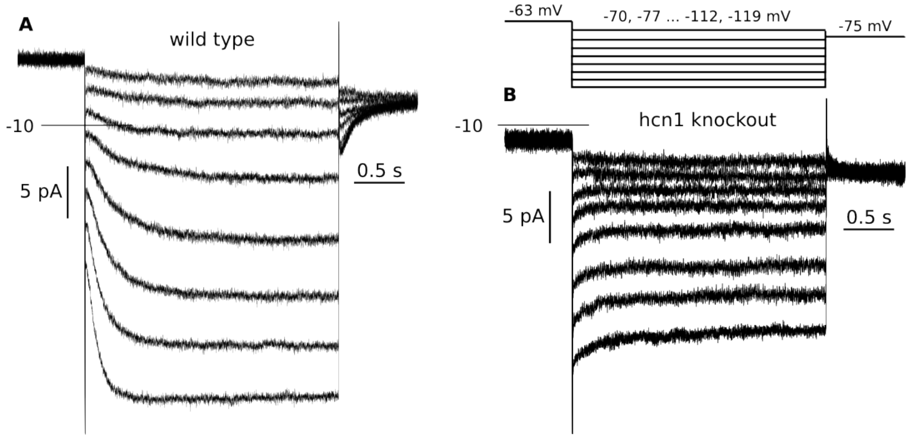

Figure 3.16: Voltage-clamp recording from rod photoreceptors in response to hyperpolarizing steps. **A**: in wild type mice the voltage- and time-dependant I_h activates upon hyperpolarization of membrane potential. **B**: in hcn1 knockout mice no I_h is activated even at most negative potential. Plotted traces are the average of respectively three and two sweeps (preliminary data).

By looking at ERG flash responses, the main visible feature in hcn1-ko animals is a prolonged recovery of the response, which happens for all the tested luminances (fig. 3.17).

Analysis of sinusoidal stimulation in the frequency domain revealed a band-pass behavior even in wild type mice, similarly to what already seen in rats (fig. 3.18 A). The most notable difference in wild type mice against rats is the preferred frequency at which the band-pass behavior reaches its maximum, around 1 Hz for rats while 2Hz in mice.

In presence of the hcn1 knockout genotype the frequency-response curve partially resembles what already seen on rats treated with HCN inhibitor; we assist to an attenuation of the response to stimuli of frequencies comprised between 0.7 and 20 Hz. (fig. 3.18 A). The attenuation is not sufficient to induce a complete shift from a band- to a low-pass mode, and by plotting data on a relative scale (fig. 3.18 B) it is seen that a band-pass profile is still present, with a peak-frequency shifted towards low frequencies and centered around 1 Hz.

On the other hand, subcutaneous administration of 20 mg/kg Ivabradine induced a more marked frequency-dependant reduction of sinusoidal ERG re-

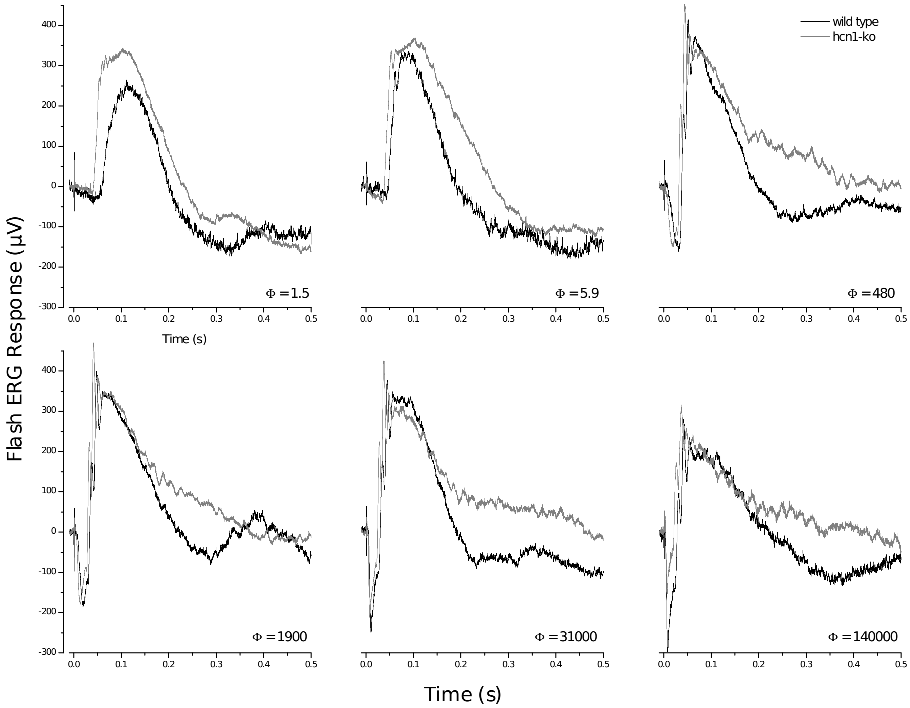

Figure 3.17: Representative example of flash ERG response in wild type and hcn1-ko mice. Note how hcn1-ko responses are prolonged with respect to wild type ones, a feature affecting the recovery phase for all the tested light intensities.

sponse like already shown in rats. The subcutaneous route of administration is expected to induce a more delayed effect than the intravenous one. In fact, by looking to heart rate, its reduction requires several tenths of minutes in order to reach its maximum, followed by a very slow recovery (see fig. 3.19 A); correspondingly, the ERG is affected maximally within the first hour from administration and slowly recovers to a shape similar to that shown by hcn1-ko mice, with a resonant peak centered on 1 Hz (see fig. 3.19 B), suggesting that recovery kinetics from this organic blocker may be different for the various HCN isoforms shaping the ERG response.

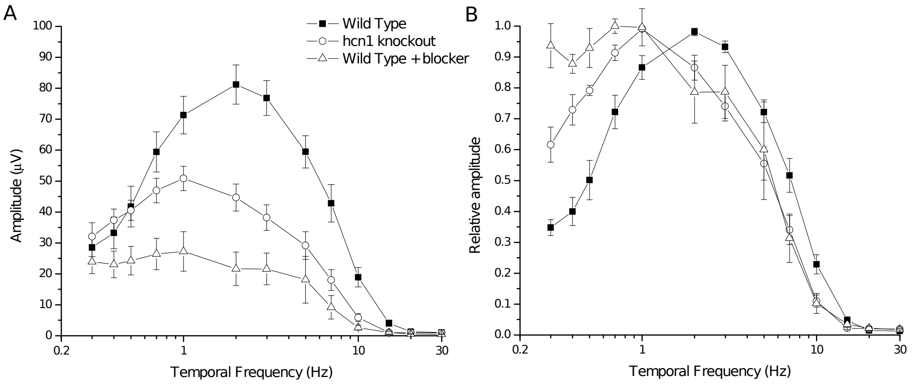

Figure 3.18: Frequency-response profiles in wild type (filled circles, n=8), hcn1-ko mice (open circles, n=8) and wild type treated with a s.c. injection of 20 mg/kg Ivabradine (open triangles, n=5); values expressed as mean±SEM. **A**: Profiles in absolute values shows an amplitude reduction for hcn1-ko for frequencies >0.5Hz, and in wild type mice treated with Ivabradine for frequencies >0.3 Hz. **B**: Relative amplitudes points out in hcn1-ko a partial preservation of band-pass properties, with a peak-frequency shifted toward 1 Hz (data normalized to maximal values for each experiment).

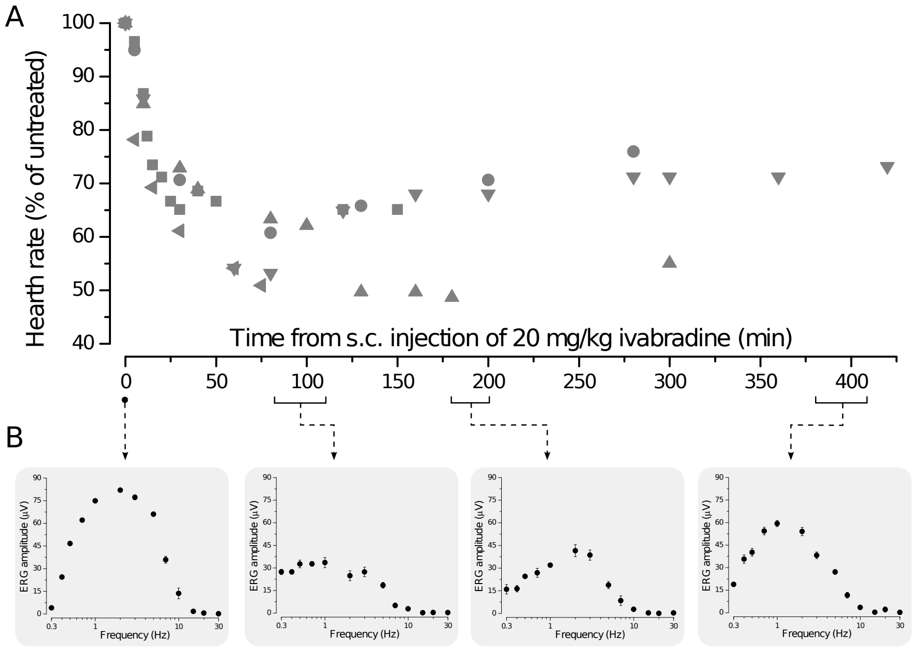

Figure 3.19: **A**: Time course of hearth rate reduction in mice, following a single subcutaneous injection of 20 mg/kg Ivabradine, collected data from each single experiment (n=5). **B**: Representative example of ERG frequency profile changes induced by the same drug administration, values expressed as mean±SEM (n variable from 5 to 25 depending upon frequency).

Chapter 4

Discussion

> *There was a man who sat each day looking out through a narrow vertical opening where a single board had been removed from a wooden fence. Each day a wild ass of the desert passed outside the fence and across the narrow opening: first the nose, then the head, the forelegs, the long brown back, the hindlegs, and lastly the tail. One day the man leaped to his feet with a light of discovery in his eyes and he shouted for all who could hear him: "It is obvious! The nose causes the tail!"*
>
> Stories of the Hidden Wisdom, from the Oral History of Rakis

4.1 Properties of RBCs in physiological conditions

As shown in results, I_h activation is associated with a band-pass behavior of the frequency response curves in RBCs. Previous papers reported an average membrane potential in darkness of -59mV [109], -60 mV [24] for mice RBC, -45 mV for rats [28]; while in this study we report an average membrane potential of -75 mV in dark adapted conditions. A couple of accountable factors suggests the membrane potential reported in literature as possibly biased toward depolarized potential with respect to the real dark-adapted value:

- The loss of rod outer segments due to mechanical disrupture of the tissue during slice preparation could keep the RBC in a depolarized state, since the damaged upstream rods experience hyperpolarization and tonically release glutamate. In support of this hypothesis we have also recorded more depolarized resting potentials of around -50/-60 mV in the early phases of this work; the membrane potential improved to -70/-80 mV as the section's morphology was finely preserved during the slicing operation and along with that we also experienced more light responses in the preparation.
- The other important factor to be taken into account is the shunt caused by the finite resistance of the seal between the pipette and the cell membrane, usually happening when performing patch onto small neurons like RBCs with input resistance in the GΩ range.

A finite seal-resistance introduces a conductance to ground in parallel to the cell's membrane, this depolarizes the cell with respect to its unperturbed state. Experiments performed on larger cells showed that the seal-resistance is quite variable, usually in a range below 50 GΩ [31] (a direct measure in mouse RBCs is quite difficult since it requires a double patch onto the same neuron). When a pipette is sealed to the membrane and held at the apparent potential V_{dark}, in steady-state conditions the sum of currents is zero (4.1):

$$\begin{aligned} I_{leak} + I_h + I_{seal} &= 0 \\ G_{leak}(V_{dark} - V_{leak}) + g_h(V_{dark})(V_{dark} - V_h) + G_{seal}(V_{dark} - 0) &= 0 \end{aligned} \tag{4.1}$$

where: V_h is the reverse potential of I_h (-34 mV), while g_h is computed from equation (2.2). The resulting true dark-adapted potential as a function of seal resistance for the apparent V_{dark} is plotted in fig.4.1.

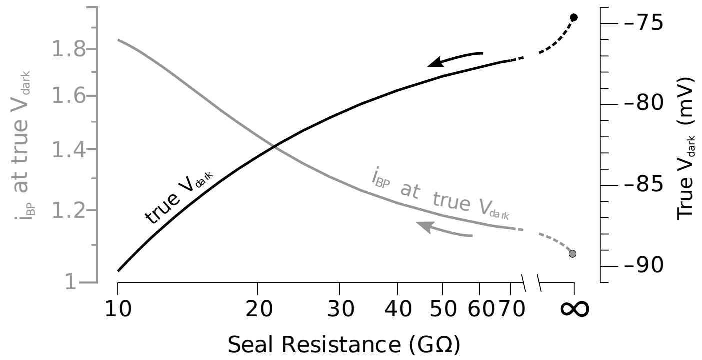

Figure 4.1: Effect of finite seal resistance on membrane potential and I_{bp}. The unperturbed dark-adapted membrane potential becomes more negative considering a finite seal resistance, in parallel the band pass index of the cell increases. V_{dark} is the apparent potential (-74.7 mV), g_h is computed using the average values G_h = 0.163 nS, $V_{1/2}$ = -91.4 mV, k_m = 6.3 mV

The effect of body temperature on I_h properties is to speed kinetics of this current along with an increment in its maximal conductance, shifting the resonant peak of the impedance profile toward higher frequencies [9].

4.2 Frequency tuning

Both rats and mice show a band-pass profile in ERG responses to sinusoidal stimulation, a feature abolished by inhibiting I_h. By looking at RBC properties, from whom originate the majority of ERG response to weak light stimuli, I_h presence is sufficient to explain the resonant behavior around the dark-adapted resting potential. The relevance of this band-pass behavior could be multiple: it contributes to counteract the inherently slowness introduced by the amplification mechanisms occurring during phototransduction and electrotonic signal spreading toward ganglion cells. The price paid for this acceleration is the loss of information occurring at low-frequency, which usually represents slow changes happening in the world around the subject, which most of times are of scarce perceptual relevance. The loss of low-frequency content, along with network convergence and amplification of the resulting signal at synaptic level, represents a way to improve the signal-over-noise ratio of the resulting signal. It also limits the propagation of noise originated inside the retina [29], which otherwise would be processed by the amplification systems. Efficacy of I_h-empowered properties for sharpening the time range useful for temporal summation could be crucial in limiting the propagation of uncorrelated signals to ganglion cells, like those occurring for example from thermal breakdown of rhodopsin. Indirect clues that these roles are played by I_h come from clinical trials of I_h inhibitors: Patients treated with these molecules in order to modulate the cardiac I_f, experience dose related side-effects on the visual system like phosphenes, stroboscopic and blurred vision. All these effects can result from the loss of I_h triggered properties at the retinal level, as summarized in fig.4.2.

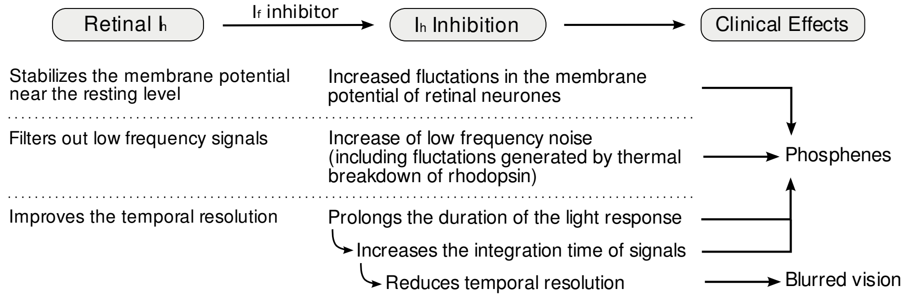

Figure 4.2: I_h implication in clinically reported side effects of I_f inhibitors

4.3 HCN subtype expression and relative role

Both in vivo and in vitro recordings show frequency tuning, is this predominantly due to a single HCN subtype? HCN1 subtype is known to be mainly expressed by rods, where these channels are involved in shaping temporal profile of the voltage response to bright flashes of light. This happens because in the dark, photoreceptors are maintained in a depolarized state, so that their membrane potential crosses I_h activation range only upon light-induced hyperpolarization. By contrary, I_h's influence in shaping temporal properties of RBC becomes less relevant as the intensity of light stimulation increases, since the membrane potential of these cells in dark adapted conditions is already in the range of I_h activation. Immunohistochemistry data provide evidence for a possible HCN2 expression at the level of RBC dendrites, in correspondence to rod synaptic terminals, although a previous study reported HCN2 presence at the level of RBC synaptic buttons [74]. An indication that HCN2 can be located in RBCs' dendrites comes also from the observation that in experiments in which the recording electrode was gently pulled until the RBC light response was abolished, also I_h was also no more present. The suggestion is that the mechanical stress on the RBC tears off the dendrites disconnecting it from rods. The possibility that HCN2 may also be expressed on horizontal cell's dendritic terminals cannot be excluded at the moment, a detailed immunostaining along with electron microscopy would probably be required to achieve the necessary spatial resolution to rule out the possibility.

A direct comparison of I_h's kinetics with other studies is unfortunately far from straight. In our experiments we experienced τ_{max}=443 ms at room temperature, while the one reported for heterologously expressed HCN1 (τ_{max}= 170 to 750 ms) and HCN2 (τ_{max}= 0.5 to 7 s). Indirect clue of isoform relevance comes from clinically reported side-effects of I_f inhibitors. These effects are reported by patients as happening especially in conditions of scarce ambient illumination, where rod-based vision is predominant. In sinusoidal ERG experiments the band-pass behavior is not fully accountable to the rod-expressed HCN1, since in hcn1-knockout mice the band-pass behavior, tough less prominent than in wild type, is still present, while HCN inhibition suppresses it completely.

4.4 Future directions

This work points out the relative importance of HCN channels in shaping the temporal properties of the retina, at least in scotopic and mesopic condition of illumination. Anyway, some major points still remain uninvestigated, most notably:

- *I_h presence and role on the cone pathway*: Immunohistochemical evidences presented in this thesis and in recent literature points out the presence of HCN channels in cones and cone-bipolar cells, in particular HCN1 and HCN3 are found cones, the latter in their pedicles, and may thus affect early cone signalling in a similar way as HCN1 affects signal processing in rods [19]. HCN3 and HCN1 are the two channel isoforms less affected by cyclic nucleotide modulation. The reason why evolution chose these isoforms to be placed in photoreceptors is yet to be investigated, a possibility could be that the role HCN channels play in photoreceptors does not require dynamical tuning that modulation provides. Alternatively, since intracellular modulation promoted by cyclic nucleotides serves mainly other features as phototransduction [33] [76], these isoforms poorly sensitive to cyclic nucleotide were selected in order to uncouple modulation of CNG and HCN channels, preferring other ways to regulate HCN channels properties like phosphoinositides [115].

- *HCN implication on long-term adaptation mechanisms:* In opposite to the expression pattern in photoreceptors, HCN isoforms expressed by retinal second-order neurons are highly modulable by cyclic nucleotides, this pathway could provide an efficient way for the retina to adapt HCN properties on the basis of several factors like: background intensity level, noise propagating from previous stations, membrane potential. Therefore a role of HCN channel in long-term adaptative processes like light- and dark-adaptation is likely but remains to be investigated.
  A long-term remodeling mechanism involving HCN channels is the possible change in their expression pattern during development, especially since some clues exists for other body districts [95]. Investigation of HCN channel distribution in wild type retina during development is becoming

more urgent, especially since the availability of knockout mice lines lacking single HCN isoforms as models for investigating the relative isoform contribution to retinal network.

- *Functional role of HCN channels in retinal ganglion cells:* Ganglion cells represent the final decision maker for the analog-to-digital conversion of the retinal signal. This makes them the ideal place to implement threshold filter and coincidence detection mechanisms capable of rejecting undesired stimuli, preventing them from proceed toward the brain. In this respect I_h may play a major role in establishing these selective processes due to its high-pass filtering properties. I_h could also come into play for explaining some noise-related features of the visual system like the presence of stochastic resonance, a mechanism already reported to happen during visual scene processing [94] [93] [83] and demonstrated to be a clever and efficient way the nature adopted to improve signal-to-ratio in other sensory systems [60].

Nomenclature

AC	Amacrine cell
ANOVA	Analysis of variance, a parametrical statistic method
Avertin	2,2,2 Tribromethanol; an injectable anesthetic agent
cAMP	Cyclic adenosine monophosphate
CBC	Cone Bipolar Cell
cGMP	Cyclic guanosine monophosphate
CNBD	Cyclic nucleotyde binding domain
CNS	Central nervous system
DMSO	Dimethyl sulfoxide; an organic solvent
DRG	Dorsal root ganglion
DST	Daylight saving time
EPSP	Excitatory post-synaptical potential
ERG	Electroretinogram
FFT	Fast fourier transform, an efficient algorithm to compute the Disctere Fourier Transform
GC	Ganglion cell
GCL	Ganglion cell layer, retinal layer containing cellular bodies of ganglion cells and displaced amacrine cells
HC	Horizontal cell
HCN	Hyperpolarization-activated cyclic nucleotide-modulated, a type of ionic channels
INL	Inner nuclear layer, retinal layer where nuclei of second-order neurons reside
IPL	Inner plexiform layer, locus of synaptical contact between second order neurons and ganglio cells
IS	Inner segment of photoreceptors

LTP	Long-term potentiation
NFL	Optic nerve fiber layer
OCT	Optimal cutting temperature, a cryoprotective agent
ONL	Outer nuclear layer, retinal layer where nuclei of photoreceptors reside
OPL	Outer plexiform layer, locus of synaptical contact between photoreceptors and second order neurons
OS	Outer segment of photoreceptors
PE	Pigmented epithelium
PIP_2	phosphatidylinositol-4,5-biphosphate
PIPES	Piperazine-N,N'-bis(2-ethanesulfonic acid); a buffering agent
PKA	Protein kinase A
RBC	Rod bipolar cell
SAN	Sinus atrial node
SD	Standard deviation
SEM	Standard error of the mean
Urethane	Diethyl carbammate; an injectable anesthetic agent
UV	Ultraviolet, light with a wavelength comprised between visible light and x-rays

Bibliography

[1] S. P. H. Alexander, A. Mathie, and J. A. Peters. Guide to receptors and channels (GRAC), 3rd edition. *Br J Pharmacol*, 153 Suppl 2:S1–209, Mar 2008. 1.2.2

[2] P. A. Anderson and R. M. Greenberg. Phylogeny of ion channels: clues to structure and function. *Comp Biochem Physiol B Biochem Mol Biol*, 129(1):17–28, May 2001. 1.2.1

[3] T. Bal and D. A. McCormick. Synchronized oscillations in the inferior olive are controlled by the hyperpolarization-activated cation current Ih. *J Neurophysiol*, 77(6):3145–3156, Jun 1997. 1.2.3

[4] D. J. Beech and S. Barnes. Characterization of a voltage-gated K+ channel that accelerates the rod response to dim light. *Neuron*, 3(5):573–581, Nov 1989. 3.1.1

[5] E. Beitz. TeXshade: shading and labeling of multiple sequence alignments using LaTeX2 epsilon. *Bioinformatics*, 16(2):135–139, Feb 2000. 1.8

[6] E. Beitz. TeXtopo: shaded membrane protein topology plots in LaTeX2 epsilon. *Bioinformatics*, 16(11):1050–1051, Nov 2000. 1.7

[7] J. S. Borer, K. Fox, P. Jaillon, G. Lerebours, and I. I. Group. Antianginal and antiischemic effects of ivabradine, an If inhibitor, in stable angina: a randomized, double-blind, multicentered, placebo-controlled trial. *Circulation*, 107(6):817–823, Feb 2003. 1.2.6

[8] A. Bucchi, M. Baruscotti, and D. DiFrancesco. Current-dependent block of rabbit sino-atrial node If channels by ivabradine. *J Gen Physiol*, 120(1):1–13, Jul 2002. 1.2.6

[9] L. Cangiano, C. Gargini, L. DellaSantina, G. C. Demontis, and L. Cervetto. High-pass filtering of input signals by the Ih current in a non-spiking neuron, the retinal rod bipolar cell. *PLoS ONE*, 2(12):e1327, 2007. 1.10, 4.1

[10] L. Cervetto, G. C. Demontis, and C. Gargini. Cellular mechanisms underlying the pharmacological induction of phosphenes. *Br J Pharmacol*, 150(4):383–390, Feb 2007. 1.2.6

[11] L. M. Chalupa and R. W. Williams, editors. *Eye, Retina, and Visual System of the mouse.* The MIT Press, 2008. 1.1.2

[12] S. R. Chaplan, H.-Q. Guo, D. H. Lee, L. Luo, C. Liu, C. Kuei, A. A. Velumian, M. P. Butler, S. M. Brown, and A. E. Dubin. Neuronal hyperpolarization-activated pacemaker channels drive neuropathic pain. *J Neurosci*, 23(4):1169–1178, Feb 2003. 1.2.3

[13] V. P. Connaughton and G. Maguire. Differential expression of voltage-gated K+ and Ca2+ currents in bipolar cells in the zebrafish retinal slice. *Eur J Neurosci*, 10(4):1350–1362, Apr 1998. 1.2.5

[14] J. Coombs, D. van der List, G.-Y. Wang, and L. M. Chalupa. Morphological properties of mouse retinal ganglion cells. *Neuroscience*, 140(1):123–136, Jun 2006. 1.1.2

[15] M. O. Cunningham, C. H. Davies, E. H. Buhl, N. Kopell, and M. A. Whittington. Gamma oscillations induced by kainate receptor activation in the entorhinal cortex in vitro. *J Neurosci*, 23(30):9761–9769, Oct 2003. 1.2.3

[16] D. M. Dacey, H.-W. Liao, B. B. Peterson, F. R. Robinson, V. C. Smith, J. Pokorny, K.-W. Yau, and P. D. Gamlin. Melanopsin-expressing ganglion cells in primate retina signal colour and irradiance and project to the LGN. *Nature*, 433(7027):749–754, Feb 2005. 1.1.2

[17] C. Dalle and J. C. Eisenach. Peripheral block of the hyperpolarization-activated cation current (Ih) reduces mechanical allodynia in animal models of postoperative and neuropathic pain. *Reg Anesth Pain Med*, 30(3):243–248, 2005. 1.2.3

[18] G. C. Demontis, C. Gargini, T. G. Paoli, and L. Cervetto. Selective HCN1 channels inhibition by ivabradine in mouse rod photoreceptors. *Invest Ophthalmol Vis Sci*, Dec 2008. 1.2.5, 1.2.6, 3.2.1

[19] G. C. Demontis, B. Longoni, U. Barcaro, and L. Cervetto. Properties and functional roles of hyperpolarization-gated currents in guinea-pig retinal rods. *J Physiol*, 515 (Pt 3):813–828, Mar 1999. 1.2.5, 3.1.1, 4.4

[20] G. C. Demontis, A. Moroni, B. Gravante, C. Altomare, B. Longoni, L. Cervetto, and D. DiFrancesco. Functional characterisation and subcellular localisation of HCN1 channels in rabbit retinal rod photoreceptors. *J Physiol*, 542(Pt 1):89–97, Jul 2002. 1.2.5, 1.10

[21] G. C. Demontis, A. Sbrana, C. Gargini, and L. Cervetto. A simple and inexpensive light source for research in visual neuroscience. *J Neurosci Methods*, 146(1):13–21, Jul 2005. 2.4.3

[22] C. T. Dickson, J. Magistretti, M. H. Shalinsky, E. Fransn, M. E. Hasselmo, and A. Alonso. Properties and role of Ih in the pacing of subthreshold oscillations in entorhinal cortex layer ii neurons. *J Neurophysiol*, 83(5):2562–2579, May 2000. 1.2.3

[23] U. C. Dräger. Observations on monocular deprivation in mice. *J Neurophysiol*, 41(1):28–42, Jan 1978. 1.3

[24] F. A. Dunn, T. Doan, A. P. Sampath, and F. Rieke. Controlling the gain of rod-mediated signals in the mammalian retina. *J Neurosci*, 26(15):3959–3970, Apr 2006. 4.1

[25] B. Ekesten and P. Gouras. Cone and rod inputs to murine retinal ganglion cells: evidence of cone opsin specific channels. *Vis Neurosci*, 22(6):893–903, 2005. 1.1.2

[26] W. El-Kholy, P. E. MacDonald, J. M. Fox, A. Bhattacharjee, T. Xue, X. Gao, Y. Zhang, J. Stieber, R. A. Li, R. G. Tsushima, and M. B. Wheeler. Hyperpolarization-activated cyclic nucleotide-gated channels in pancreatic beta-cells. *Mol Endocrinol*, 21(3):753–764, Mar 2007. 1.2.3

[27] EMEA. European Public Assessment Report (EPAR) for Procoralan (ivabradine). Technical report, European Medicines Agency, 2005. 3.2.1

[28] T. Euler and R. H. Masland. Light-evoked responses of bipolar cells in a mammalian retina. *J Neurophysiol*, 83(4):1817–1829, Apr 2000. 4.1

[29] G. D. Field, A. P. Sampath, and F. Rieke. Retinal processing near absolute threshold: from behavior to mechanism. *Annu Rev Physiol*, 67:491–514, 2005. 4.2

[30] A. Fisahn, M. Yamada, A. Duttaroy, J.-W. Gan, C.-X. Deng, C. J. McBain, and J. Wess. Muscarinic induction of hippocampal gamma oscillations requires coupling of the M1 receptor to two mixed cation currents. *Neuron*, 33(4):615–624, Feb 2002. 1.2.3

[31] R. Fischmeister, R. K. Ayer, and R. L. DeHaan. Some limitations of the cell-attached patch clamp technique: a two-electrode analysis. *Pflugers Arch*, 406(1):73–82, Jan 1986. 4.1

[32] S. G. A. Frère, M. Kuisle, and A. Lüthi. Regulation of recombinant and native hyperpolarization-activated cation channels. *Mol Neurobiol*, 30(3):279–305, Dec 2004. 1.2.2

[33] R. E. Furman and J. C. Tanaka. Photoreceptor channel activation: interaction between cAMP and cGMP. *Biochemistry*, 28(7):2785–2788, Apr 1989. 4.4

[34] B. Fyk-Kolodziej and R. G. Pourcho. Differential distribution of hyperpolarization - activated and cyclic nucleotide - gated channels in cone bipolar cells of the rat retina. *J Comp Neurol*, 501(6):891–903, Apr 2007. 1.2.5

[35] C. Gargini, G. C. Demontis, S. Bisti, and L. Cervetto. Effects of blocking the hyperpolarization-activated current (Ih) on the cat electroretinogram. *Vision Res*, 39(10):1767–1774, May 1999. 1.2.6, 1.2.6

[36] S. Gasparini and D. DiFrancesco. Action of the hyperpolarization-activated current (Ih) blocker ZD 7288 in hippocampal CA1 neurons. *Pflugers Arch*, 435(1):99–106, Dec 1997. 1.2.6

[37] K. K. Ghosh, S. Bujan, S. Haverkamp, A. Feigenspan, and H. Wässle. Types of bipolar cells in the mouse retina. *J Comp Neurol*, 469(1):70–82, Jan 2004. 1.4

[38] B. Gravante, A. Barbuti, R. Milanesi, I. Zappi, C. Viscomi, and D. DiFrancesco. Interaction of the pacemaker channel HCN1 with filamin A. *J Biol Chem*, 279(42):43847–43853, Oct 2004. 1.2.1

[39] J. S. Haas, A. D. Dorval, and J. A. White. Contributions of Ih to feature selectivity in layer ii stellate cells of the entorhinal cortex. *J Comput Neurosci*, 22(2):161–171, Apr 2007. 1.2.3

[40] N. C. Harris and A. Constanti. Mechanism of block by ZD 7288 of the hyperpolarization-activated inward rectifying current in guinea pig substantia nigra neurons in vitro. *J Neurophysiol*, 74(6):2366–2378, Dec 1995. 1.2.6

[41] E. Hartveit. Reciprocal synaptic interactions between rod bipolar cells and amacrine cells in the rat retina. *J Neurophysiol*, 81(6):2923–2936, Jun 1999. 3.1.1

[42] S. Hattar, H. W. Liao, M. Takao, D. M. Berson, and K. W. Yau. Melanopsin-containing retinal ganglion cells: architecture, projections, and intrinsic photosensitivity. *Science*, 295(5557):1065–1070, Feb 2002. 1.1.2

[43] S. Herrmann, J. Stieber, G. Stöckl, F. Hofmann, and A. Ludwig. HCN4 provides a 'depolarization reserve' and is not required for heart rate acceleration in mice. *EMBO J*, 26(21):4423–4432, Oct 2007. 1.2.4, 1.9

[44] E. Hoesl, J. Stieber, S. Herrmann, S. Feil, E. Tybl, F. Hofmann, R. Feil, and A. Ludwig. Tamoxifen-inducible gene deletion in the cardiac conduction system. *J Mol Cell Cardiol*, 45(1):62–69, Jul 2008. 1.2.4

[45] A. Hughes. A schematic eye for the rat. *Vision Res*, 19(5):569–588, 1979. 1.3

[46] B. Hutcheon, R. M. Miura, and E. Puil. Models of subthreshold membrane resonance in neocortical neurons. *J Neurophysiol*, 76(2):698–714, Aug 1996. 2.2.7

[47] B. Hutcheon, R. M. Miura, and E. Puil. Subthreshold membrane resonance in neocortical neurons. *J Neurophysiol*, 76(2):683–697, Aug 1996. 1.2.3

[48] B. Hutcheon, R. M. Miura, Y. Yarom, and E. Puil. Low-threshold calcium current and resonance in thalamic neurons: a model of frequency preference. *J Neurophysiol*, 71(2):583–594, Feb 1994. 2.2.7

[49] B. Hutcheon and Y. Yarom. Resonance, oscillation and the intrinsic frequency preferences of neurons. *Trends Neurosci*, 23(5):216–222, May 2000. 1.2.3

[50] E. Ivanova and F. Müller. Retinal bipolar cell types differ in their inventory of ion channels. *Vis Neurosci*, 23(2):143–154, 2006. 1.10, 1.2.5, 3.1.1

[51] H. A. Jackson, C. R. Marshall, and E. A. Accili. Evolution and structural diversification of hyperpolarization-activated cyclic nucleotide-gated channel genes. *Physiol Genomics*, 29(3):231–245, May 2007. 1.2.1

[52] C. J. Jeon, E. Strettoi, and R. H. Masland. The major cell populations of the mouse retina. *J Neurosci*, 18(21):8936–8946, Nov 1998. 1.1.2, 1.5

[53] Y.-Q. Jiang, Q. Sun, H.-Y. Tu, and Y. Wan. Characteristics of HCN channels and their participation in neuropathic pain. *Neurochem Res*, 33(10):1979–1989, Oct 2008. 1.2.3

[54] A. Kaneko and M. Tachibana. A voltage-clamp analysis of membrane currents in solitary bipolar cells dissociated from carassius auratus. *J Physiol*, 358:131–152, Jan 1985. 1.2.5

[55] K. Kimura, J. Kitano, Y. Nakajima, and S. Nakanishi. Hyperpolarization-activated, cyclic nucleotide-gated HCN2 cation channel forms a protein assembly with multiple neuronal scaffold proteins in distinct modes of protein-protein interaction. *Genes Cells*, 9(7):631–640, Jul 2004. 1.2.1

[56] G. C. Knop, M. W. Seeliger, F. Thiel, A. Mataruga, U. B. Kaupp, C. Friedburg, N. Tanimoto, and F. Müller. Light responses in the mouse retina are prolonged upon targeted deletion of the hcn1 channel gene. *Eur J Neurosci*, 28(11):2221–2230, Dec 2008. 1.10

[57] A. Koizumi, T. C. Jakobs, and R. H. Masland. Inward rectifying currents stabilize the membrane potential in dendrites of mouse amacrine cells: patch-clamp recordings and single-cell RT-PCR. *Mol Vis*, 10:328–340, May 2004. 1.10, 1.2.5

[58] S. C. Lee and A. T. Ishida. Ih without Kir in adult rat retinal ganglion cells. *J Neurophysiol*, 97(5):3790–3799, May 2007. 1.2.5

[59] D. R. Linden, K. A. Sharkey, and G. M. Mawe. Enhanced excitability of myenteric AH neurones in the inflamed guinea-pig distal colon. *J Physiol*, 547(Pt 2):589–601, Mar 2003. 1.2.3

[60] J. F. Lindner, M. Bennett, and K. Wiesenfeld. Potential energy landscape and finite-state models of array-enhanced stochastic resonance. *Phys Rev E Stat Nonlin Soft Matter Phys*, 73(3 Pt 1):031107, Mar 2006. 4.4

[61] A. Ludwig, T. Budde, J. Stieber, S. Moosmang, C. Wahl, K. Holthoff, A. Langebartels, C. Wotjak, T. Munsch, X. Zong, S. Feil, R. Feil, M. Lancel, K. R. Chien, A. Konnerth, H.-C. Pape, M. Biel, and F. Hofmann. Absence epilepsy and sinus dysrhythmia in mice lacking the pacemaker channel HCN2. *EMBO J*, 22(2):216–224, Jan 2003. 1.2.4, 1.2.6

[62] A. Ludwig, X. Zong, M. Jeglitsch, F. Hofmann, and M. Biel. A family of hyperpolarization-activated mammalian cation channels. *Nature*, 393(6685):587–591, Jun 1998. 1.2.1

[63] A. Ludwig, X. Zong, J. Stieber, R. Hullin, F. Hofmann, and M. Biel. Two pacemaker channels from human heart with profoundly different activation kinetics. *EMBO J*, 18(9):2323–2329, May 1999. 1.2.1

[64] A. L. Lyubarsky, L. L. Daniele, and E. N. Pugh. From candelas to photoisomerizations in the mouse eye by rhodopsin bleaching in situ and the light-rearing dependence of the major components of the mouse ERG. *Vision Res*, 44(28):3235–3251, Dec 2004. 2.4.3

[65] A. L. Lyubarsky and E. N. Pugh. Recovery phase of the murine rod photoresponse reconstructed from electroretinographic recordings. *J Neurosci*, 16(2):563–571, Jan 1996. 2.4.3

[66] Y.-P. Ma, J. Cui, H.-J. Hu, and Z.-H. Pan. Mammalian retinal bipolar cells express inwardly rectifying K+ currents (IKir) with a different distribution than that of Ih. *J Neurophysiol*, 90(5):3479–3489, Nov 2003. 1.2.5

[67] R. Maccarone, G. Izzizzari, C. Gargini, L. Cervetto, and S. Bisti. The impact of organic inhibitors of the hyperpolarization activated current (Ih) on the electroretinogram (ERG) of rodents. *Arch Ital Biol*, 142(2):95–103, Mar 2004. 1.2.6

[68] R. Mader, A. Schneider, S. Feil, R. Feil, F. Hofmann, and M. Biel. Genetic deletion of the HCN3 pacemaker channel in mice. *Naunyn-Schmiedebergs Arch Pharmacol*, 367:339, 2003. 1.2.4

[69] J. C. Magee. Dendritic hyperpolarization-activated currents modify the integrative properties of hippocampal CA1 pyramidal neurons. *J Neurosci*, 18(19):7613–7624, Oct 1998. 1.2.3

[70] J. C. Magee. Dendritic Ih normalizes temporal summation in hippocampal CA1 neurons. *Nat Neurosci*, 2(9):848, Sep 1999. 1.2.3

[71] B. Marcelin, L. Chauvière, A. Becker, M. Migliore, M. Esclapez, and C. Bernard. h channel-dependent deficit of theta oscillation resonance and phase shift in temporal lobe epilepsy. *Neurobiol Dis*, Dec 2008. 1.2.6

[72] C. Miller. An overview of the potassium channel family. *Genome Biol*, 1(4):1–5, 2000. 1.2.1, 1.6

[73] S. Moosmang, M. Biel, F. Hofmann, and A. Ludwig. Differential distribution of four hyperpolarization-activated cation channels in mouse brain. *Biol Chem*, 380(7-8):975–980, 1999. 1.2.3

[74] F. Müller, A. Scholten, E. Ivanova, S. Haverkamp, E. Kremmer, and U. B. Kaupp. HCN channels are expressed differentially in retinal bipolar cells and concentrated at synaptic terminals. *Eur J Neurosci*, 17(10):2084–2096, May 2003. 1.2.5, 1.10, 1.2.5, 3.1.4, 4.3

[75] S. S. Nikonov, R. Kholodenko, J. Lem, and E. N. Pugh. Physiological features of the S- and M-cone photoreceptors of wild-type mice from single-cell recordings. *J Gen Physiol*, 127(4):359–374, Apr 2006. 1.1.2

[76] I. Nir, J. M. Harrison, R. Haque, M. J. Low, D. K. Grandy, M. Rubinstein, and P. M. Iuvone. Dysfunctional light-evoked regulation of cAMP in photoreceptors and abnormal retinal adaptation in mice lacking dopamine D4 receptors. *J Neurosci*, 22(6):2063–2073, Mar 2002. 4.4

[77] M. F. Nolan, G. Malleret, J. T. Dudman, D. L. Buhl, B. Santoro, E. Gibbs, S. Vronskaya, G. Buzsáki, S. A. Siegelbaum, E. R. Kandel, and A. Morozov. A behavioral role for dendritic integration: HCN1 channels constrain spatial memory and plasticity at inputs to distal dendrites of CA1 pyramidal neurons. *Cell*, 119(5):719–732, Nov 2004. 1.2.3

[78] M. F. Nolan, G. Malleret, K. H. Lee, E. Gibbs, J. T. Dudman, B. Santoro, D. Yin, R. F. Thompson, S. A. Siegelbaum, E. R. Kandel, and A. Morozov. The hyperpolarization-activated HCN1 channel is important for motor learning and neuronal integration by cerebellar Purkinje cells. *Cell*, 115(5):551–564, Nov 2003. 1.2.3, 1.2.4

[79] T. Notomi and R. Shigemoto. Immunohistochemical localization of Ih channel subunits, HCN1-4, in the rat brain. *J Comp Neurol*, 471(3):241–276, Apr 2004. 1.2.3

[80] H. Oi, G. J. Partida, S. C. Lee, and A. T. Ishida. HCN4-like immunoreactivity in rat retinal ganglion cells. *Vis Neurosci*, 25(1):95–102, 2008. 3.1.4

[81] C. W. Oyster. The analysis of image motion by the rabbit retina. *J Physiol*, 199(3):613–635, Dec 1968. 1.1.2

[82] Z. H. Pan. Differential expression of high- and two types of low-voltage-activated calcium currents in rod and cone bipolar cells of the rat retina. *J Neurophysiol*, 83(1):513–527, Jan 2000. 3.1.1

[83] A. Patel and B. Kosko. Stochastic resonance in noisy spiking retinal and sensory neuron models. *Neural Netw*, 18(5-6):467–478, 2005. 4.4

[84] V. Pignatelli and E. Strettoi. Bipolar cells of the mouse retina: a gene gun, morphological study. *J Comp Neurol*, 476(3):254–266, Aug 2004. 1.4

[85] N. P. Poolos, M. Migliore, and D. Johnston. Pharmacological upregulation of h-channels reduces the excitability of pyramidal neuron dendrites. *Nat Neurosci*, 5(8):767–774, Aug 2002. 1.2.2, 1.2.6

[86] K. L. Powell, C. Ng, T. J. O'Brien, S. H. Xu, D. A. Williams, S. J. Foote, and C. A. Reid. Decreases in HCN mRNA expression in the hippocampus after kindling and status epilepticus in adult rats. *Epilepsia*, 49(10):1686–1695, Oct 2008. 1.2.6

[87] E. Puil, B. Gimbarzevsky, and R. M. Miura. Quantification of membrane properties of trigeminal root ganglion neurons in guinea pigs. *J Neurophysiol*, 55(5):995–1016, May 1986. 2.2.6

[88] S. Remtulla and P. E. Hallett. A schematic eye for the mouse, and comparisons with the rat. *Vision Res*, 25(1):21–31, 1985. 1.1.2

[89] J. L. Sánchez-Alonso, J. V. Halliwell, and A. Colino. ZD 7288 inhibits T-type calcium current in rat hippocampal pyramidal cells. *Neurosci Lett*, 439(3):275–280, Jul 2008. 1.2.6

[90] B. Santoro, S. Chen, A. Luthi, P. Pavlidis, G. P. Shumyatsky, G. R. Tibbs, and S. A. Siegelbaum. Molecular and functional heterogeneity of hyperpolarization-activated pacemaker channels in the mouse CNS. *J Neurosci*, 20(14):5264–5275, Jul 2000. 1.2.3

[91] T.-O. Satoh and M. Yamada. Multiple inhibitory effects of zatebradine (UL-FS 49) on the electrophysiological properties of retinal rod photoreceptors. *Pflugers Arch*, 443(4):532–540, Feb 2002. 1.2.6

[92] M. Semo, M. M. noz Llamosas, R. G. Foster, and G. Jeffery. Melanopsin (Opn4) positive cells in the cat retina are randomly distributed across the ganglion cell layer. *Vis Neurosci*, 22(1):111–116, 2005. 1.1.2

[93] R. A. Shiells and G. Falk. Potentiation of 'on' bipolar cell flash responses by dim background light and cGMP in dogfish retinal slices. *J Physiol*, 542(Pt 1):211–220, Jul 2002. 4.4

[94] E. Simonotto, M. Riani, C. Seife, M. Roberts, J. Twitty, and F. Moss. Visual perception of stochastic resonance. *Phys Rev Lett*, 78(6):1186–1189, Feb 1997. 4.4

[95] J. Stieber, S. Herrmann, S. Feil, J. Löster, R. Feil, M. Biel, F. Hofmann, and A. Ludwig. The hyperpolarization-activated channel HCN4 is required for the generation of pacemaker action potentials in the embryonic heart. *Proc Natl Acad Sci U.S.A.*, 100(25):15235–15240, Dec 2003. 1.2.4, 4.4

[96] S. Sulfi and A. D. Timmis. Ivabradine – the first selective sinus node If channel inhibitor in the treatment of stable angina. *Int J Clin Pract*, 60(2):222–228, Feb 2006. 1.2.6

[97] W. Sun, N. Li, and S. He. Large-scale morphological survey of mouse retinal ganglion cells. *J Comp Neurol*, 451(2):115–126, Sep 2002. 1.1.2

[98] A. Szél and P. Röhlich. Two cone types of rat retina detected by anti-visual pigment antibodies. *Exp Eye Res*, 55(1):47–52, Jul 1992. 1.1.2

[99] A. Szél, P. Rhlich, A. R. Caffé, B. Juliusson, G. Aguirre, and T. V. Veen. Unique topographic separation of two spectral classes of cones in the mouse retina. *J Comp Neurol*, 325(3):327–342, Nov 1992. 1.1.2

[100] T. Tabata and A. T. Ishida. Transient and sustained depolarization of retinal ganglion cells by Ih. *J Neurophysiol*, 75(5):1932–1943, May 1996. 1.2.5

[101] N. Tran, C. Proenza, V. Macri, F. Petigara, E. Sloan, S. Samler, and E. A. Accili. A conserved domain in the NH2 terminus important for assembly and functional expression of pacemaker channels. *J Biol Chem*, 277(46):43588–43592, Nov 2002. 1.2.1

[102] Y. Tsukamoto, K. Morigiwa, M. Ueda, and P. Sterling. Microcircuits for night vision in mouse retina. *J Neurosci*, 21(21):8616–8623, Nov 2001. 1.1.2

[103] D. Ulrich. Dendritic resonance in rat neocortical pyramidal cells. *J Neurophysiol*, 87(6):2753–2759, Jun 2002. 1.2.3

[104] M. Wang, B. P. Ramos, C. D. Paspalas, Y. Shu, A. Simen, A. Duque, S. Vijayraghavan, A. Brennan, A. Dudley, E. Nou, J. A. Mazer, D. A. McCormick, and A. F. T. Arnsten. Alpha2A-adrenoceptors strengthen working memory networks by inhibiting cAMP-HCN channel signaling in prefrontal cortex. *Cell*, 129(2):397–410, Apr 2007. 1.2.3

[105] W.-T. Wang, Y.-H. Wan, J.-L. Zhu, G.-S. Lei, Y.-Y. Wang, P. Zhang, and S.-J. Hu. Theta-frequency membrane resonance and its ionic mechanisms in rat subicular pyramidal neurons. *Neuroscience*, 140(1):45–55, Jun 2006. 1.2.3

[106] H. Wässle, C. Puller, F. Müller, and S. Haverkamp. Cone contacts, mosaics, and territories of bipolar cells in the mouse retina. *J Neurosci*, 29(1):106–117, Jan 2009. 3.1.4

[107] S. Weng, W. Sun, and S. He. Identification of ON-OFF direction-selective ganglion cells in the mouse retina. *J Physiol*, 562(Pt 3):915–923, Feb 2005. 1.1.2

[108] L. P. Wollmuth and B. Hille. Ionic selectivity of Ih channels of rod photoreceptors in tiger salamanders. *J Gen Physiol*, 100(5):749–765, Nov 1992. 1.2.2, 2.2.5

[109] S. M. Wu, F. Gao, and J.-J. Pang. Synaptic circuitry mediating light-evoked signals in dark-adapted mouse retina. *Vision Res*, 44(28):3277–3288, Dec 2004. 4.1

[110] J. Xiao, Y. Cai, J. Yen, M. Steffen, D. A. Baxter, A. Feigenspan, and D. Marshak. Voltage-clamp analysis and computational model of dopaminergic neurons from mouse retina. *Vis Neurosci*, 21(6):835–849, 2004. 1.2.5

[111] J. Xiao, T. V. Nguyen, K. Ngui, P. J. L. M. Strijbos, I.-S. Selmer, C. B. Neylon, and J. B. Furness. Molecular and functional analysis of hyperpolarisation-activated nucleotide-gated (HCN) channels in the enteric nervous system. *Neuroscience*, 129(3):603–614, 2004. 1.2.3

[112] F. H. Yu, V. Yarov-Yarovoy, G. A. Gutman, and W. A. Catterall. Overview of molecular relationships in the voltage-gated ion channel superfamily. *Pharmacol Rev*, 57(4):387–395, Dec 2005. 1.2.1

[113] Y. Zhang, N. Zhang, A. V. Gyulkhandanyan, E. Xu, H. Y. Gaisano, M. B. Wheeler, and Q. Wang. Presence of functional hyperpolarisation-activated cyclic nucleotide-gated channels in clonal alpha cell lines and rat islet alpha cells. *Diabetologia*, 51(12):2290–2298, Dec 2008. 1.2.3

[114] Z.-Y. Zhou, Q.-F. Wan, P. Thakur, and R. Heidelberger. Capacitance measurements in the mouse rod bipolar cell identify a pool of releasable synaptic vesicles. *J Neurophysiol*, 96(5):2539–2548, Nov 2006. 2.2.7

[115] G. Zolles, N. Klöcker, D. Wenzel, J. Weisser-Thomas, B. K. Fleischmann, J. Roeper, and B. Fakler. Pacemaking by HCN channels requires interaction with phosphoinositides. *Neuron*, 52(6):1027–1036, Dec 2006. 1.2.2, 4.4

Acknowledgments

This doctoral thesis could not be considered complete before I have the possibility to thank the people who carried me across this intense three years-long voyage:

Thanks to Prof. Luigi Cervetto and Prof. Claudia Gargini for continuously supporting me and my studies with your invaluable professional skills and human touch; it is a privilege to work under your supervision.

My deepest thanks goes to Lorenzo Cangiano, Ilaria Piano, Antonella Asta and Sabrina Asteriti. Every single word laid down on these otherwise pallid sheets of paper is especially the fruit of your constant efforts and perseverance with me, of your support, critical point of view, but mostly of the passion you daily put in your work that inevitably infects everyone surround you.

A warmful thank to Mariangela Alaimo, Marco Perelli and Ilaria Mucci for their critical review of the manuscript. It is an exquisite pleasure for me having such a solid reference point as your friendship.

A special thank goes to Monica Meini, who carefully chose the opening illustration and helped me during hard days. Thanks for making me hear that distant crying child again.